Article

Cell Reports

cKit Lineage Hemogenic Endothelium-Derived Cells Contribute to Mesenteric Lymphatic Vessels

Graphical Abstract

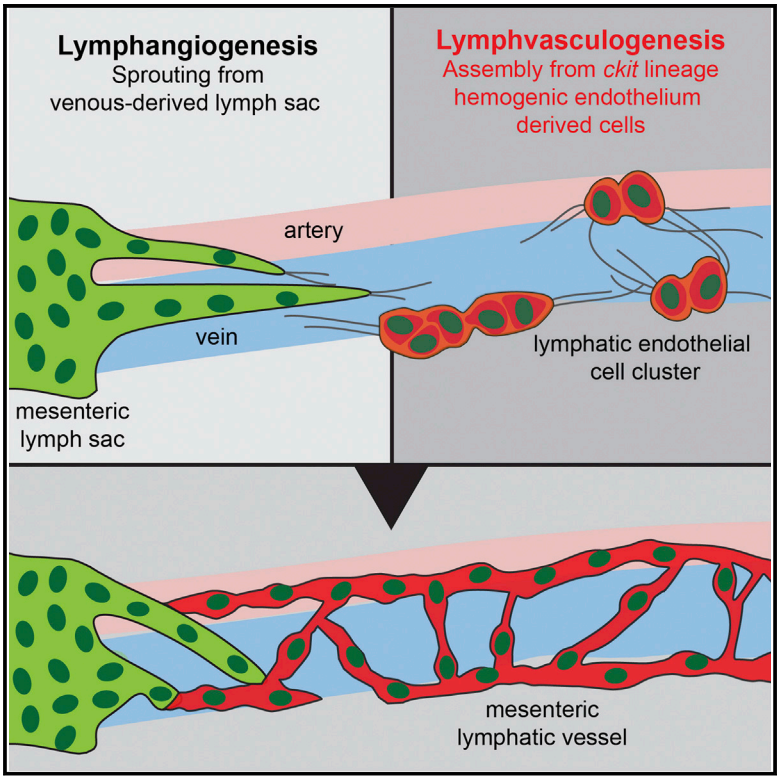

Highlights

- VEGFR-3/PI3K signaling regulates organ-specific mesenteric lymphatic development
- Different lymphatic vascular beds have different origins
- Hemogenic endothelium-derived cells contribute to mesenteric lymphatic vessels
- Mesenteric lymphatic vessels develop by a process defined as lymphvasculogenesis

Authors

Lukas Stanczuk, Ines Martinez-Corral, ..., Mariona Graupera, Taija Mäkinen

Correspondence

taija.makinen@igp.uu.se

In Brief

Stanczuk et al. show that lymphatic vessels in different organs are of different origins. Lymphatic vessels in the mesentery develop from hemogenic endothelium-derived cells, unlike lymphatic vessels in other organs that form via sprouting from veins.

Stanczuk et al., 2015, Cell Reports *10*, 1708–1721
March 17, 2015
http://dx.doi.org/10.1016/j.celrep.2015.02.026

CellPress

OPEN ACCESS
CellPress

Cell Reports
Article

cKit Lineage Hemogenic Endothelium-Derived Cells Contribute to Mesenteric Lymphatic Vessels

Lukas Stanczuk,[1,2] Ines Martinez-Corral,[1,2] Maria H. Ulvmar,[1] Yang Zhang,[1] Bàrbara Laviña,[1] Marcus Fruttiger,[4] Ralf H. Adams,[5] Dieter Saur,[6,7] Christer Betsholtz,[1,3] Sagrario Ortega,[8] Kari Alitalo,[9] Mariona Graupera,[10] and Taija Mäkinen[1,2,*]

[1]The Beijer Laboratory, Department of Immunology, Genetics and Pathology, Uppsala University, Dag Hammarskjöldsväg 20, 752 85 Uppsala, Sweden
[2]Lymphatic Development Laboratory, Cancer Research UK London Research Institute (LRI), 44 Lincoln's Inn Fields, London WC2A 3LY, UK
[3]Division of Vascular Biology, Department of Medical Biochemistry and Biophysics, Karolinska Institute, Scheeles Väg 2, 171 77 Stockholm, Sweden
[4]UCL Institute of Ophthalmology, University College London (UCL), 11-43 Bath Street, London EC1V 9EL, UK
[5]Department of Tissue Morphogenesis, Max Planck Institute for Molecular Biomedicine, and Faculty of Medicine, University of Münster, 48149 Münster, Germany
[6]Department of Internal Medicine 2, Klinikum Rechts der Isar, Technische Universität München, Ismaningerstrasse 22, 81675 Munich, Germany
[7]German Cancer Consortium (DKTK) and German Cancer Research Center (DKFZ), Im Neuenheimer Feld 280, 69120 Heidelberg, Germany
[8]Biotechnology Programme, Spanish National Cancer Research Centre, Melchor Fernández Almagro 3, 28029 Madrid, Spain
[9]Wihuri Research Institute and Translational Cancer Biology Program, Biomedicum Helsinki, University of Helsinki, Haartmaninkatu 8, 00014 Helsinki, Finland
[10]Vascular Signalling Lab, IDIBELL, 3a planta - Gran Via de l'Hospitalet 199, L'Hospitalet de Llobregat, 08908 Barcelona, Spain
*Correspondence: taija.makinen@igp.uu.se
http://dx.doi.org/10.1016/j.celrep.2015.02.026

SUMMARY

Pathological lymphatic diseases mostly affect vessels in specific tissues, yet little is known about organ-specific regulation of the lymphatic vasculature. Here, we show that the vascular endothelial growth factor receptor 3 (VEGFR-3)/p110α PI3-kinase signaling pathway is selectively required for the formation of mesenteric lymphatic vasculature. Using genetic lineage tracing, we demonstrate that part of the mesenteric lymphatic vasculature develops from *cKit* lineage cells of hemogenic endothelial origin through a process we define as lymphvasculogenesis. This is contrary to the current dogma that all mammalian lymphatic vessels form by sprouting from veins. Our results reveal vascular-bed-specific differences in the origin and mechanisms of vessel formation, which may critically underlie organ-specific manifestation of lymphatic dysfunction in disease. The progenitor cells identified in this study may be exploited to restore lymphatic function following cancer surgery, lymphedema, or tissue trauma.

INTRODUCTION

The circulatory system is composed of hierarchical networks of blood and lymphatic vessels with specific features serving their specialized functions. Structural and functional differences among arteries, capillaries, veins, and lymphatic vessels are reflected by unique transcriptional signatures within endothelial cells lining these vessels (Aird, 2007a, b). In addition, vascular beds of different organs show remarkable specialization that allows them to fulfill the functional needs of each organ. For example, capillary beds of the kidney and the brain show organotypic features that reflect their opposite roles in controlling passage of solutes between the tissue and the blood. Endothelial cells of the kidney glomeruli have fenestrae for the filtration of blood, while those of the blood-brain barrier display specialized tight junctions and a low rate of vesicular transcytosis, thus forming a barrier that seals the central nervous system (Aird, 2007b; Engelhardt and Liebner, 2014). Gene expression profiling of microvascular endothelial cells from different organs revealed unique transcriptional signatures for transcription factors and adhesion molecules (Nolan et al., 2013). In addition, tissue-specific endothelial cells produce a unique repertoire of angiocrine growth factors and chemokines, which indicates an important role for the vasculature in organ development, homeostasis, and regeneration (Butler et al., 2010a, 2010b; Ding et al., 2010; Kusumbe et al., 2014; Nolan et al., 2013).

Embryonic blood vessels form via two fundamentally different mechanisms, de novo formation of vessels from endothelial progenitors (vasculogenesis) and sprouting of vessels from pre-existing ones (angiogenesis). In contrast, mammalian lymphatic vasculature is thought to form exclusively through an angiogenic process involving endothelial cell sprouting from the veins (lymphangiogenesis) (Srinivasan et al., 2007). Upon exit from the vein, the differentiated lymphatic endothelial cells (LECs) form the first primitive lymphatic structures called lymph sacs, from which lymphatic vessels of peripheral organs are formed via

further sprouting. Although much has been learned about the general mechanisms of blood and lymphatic vessel formation, organ-specific vascular development and specialization remain poorly understood. Extracellular signals provided by the specific tissue microenvironment are likely to play a key role in this process, but cell-intrinsic genetic mechanisms also are involved. For example, canonical Wnt7a/Wnt7b signaling was shown to control organ-specific formation of the CNS vasculature, while Mfsd2a specifically regulates the formation of the blood-brain barrier (Armulik et al., 2010; Ben-Zvi et al., 2014; Stenman et al., 2008).

Dysfunction of lymphatic vasculature recently has been linked to a number of human pathologies, including inflammation, obesity, and cardiovascular disease (Alitalo, 2011). A prominent clinical consequence of the failure of the lymphatic system, caused by a genetic defect or damage following surgery or trauma, is tissue swelling or lymphedema. Notably, several hereditary lymphedemas are characterized by defects that affect specific tissues or organs. For example, in Milroy disease and lymphedema-distichiasis syndrome, which are caused by mutations in genes encoding VEGFR-3 and FOXC2, respectively, lymphedema is restricted to the lower limbs (Connell et al., 2013). In other syndromes, it also can occur in hands or genitalia, or manifest as a generalized lymphatic dysplasia with a degree of systemic involvement, such as intestinal or pulmonary lymphangiectasia (Connell et al., 2013). Molecular mechanisms underlying organ-specific manifestation of lymphatic dysfunction are not characterized, yet this knowledge is instrumental in designing therapeutic strategies for lymphedema and other lymphatic disorders, which are currently lacking.

Here we identify a hitherto unrecognized mechanism by which lymphatic vascular morphogenesis is regulated in an organ-specific manner. We show that VEGFR-3/PI3K signaling is selectively required for the formation of mesenteric lymphatic vessels. Using genetic lineage tracing, we further demonstrate that, contrary to current belief that all mammalian lymphatic vessels form by sprouting from veins, part of the mesenteric lymphatic vasculature forms from non-venous-derived progenitors of hemogenic endothelial origin.

RESULTS

VEGFR-3/PI3K Signaling Is Selectively Required for Mesenteric Lymphatic Vessel Development

To understand organ-specific mechanisms of lymphangiogenesis, we investigated the requirement of the key lymphangiogenic growth factor receptor, VEGFR-3, in the development of different lymphatic vascular beds. Since homozygous deletion of *Vegfr3* is expected to lead to loss or severe hypoplasia of lymphatic vessels in all organs, we instead analyzed hypomorphs with partial and selective deficiency of VEGFR-3 signaling via the PI3-kinase pathway. For this purpose, we generated mice carrying single functional copies of genes encoding VEGFR-3 and the p110α catalytic subunit of PI3K, which is the key downstream effector of VEGFR signaling in blood and lymphatic endothelia (Graupera et al., 2008; Gupta et al., 2007; Vanhaesebroeck et al., 2010). Mice carrying a heterozygous *Vegfr3* null (*Vegfr3*$^{lz/+}$) or a heterozygous kinase-dead *PIK3CA* allele (denoted as *p110α*$^{D933A/+}$) developed into adulthood and showed normal lymphatic vasculature (Dumont et al., 1998; Graupera et al., 2008; data not shown). In contrast, double-heterozygous *Vegfr3*$^{lz/+}$;*p110α*$^{D933A/+}$ animals died perinatally and exhibited vascular defects characterized by near absence of mesenteric lymphatic vessels and leakage of chylous fluid (Figures S1A–S1C). While in control mice each artery-vein pair extending from the mesenteric root to the intestine is accompanied by a lymphatic vessel (Figure S1C; data not shown), only a rare and often truncated lymphatic vessel could be found in neonatal *Vegfr3*$^{lz/+}$;*p110α*$^{D933A/+}$ mice at P0–P4 (Figures S1C, 1A, and 1B). The few lymphatic vessels that developed in the mutant mesentery were dilated and exhibited abnormal expression of LYVE-1, which was downregulated in mesenteric vessels of control neonatal mice (Figure S1C).

To exclude the possibility that the lymphatic phenotype was due to growth retardation, we analyzed mice at embryonic stages when *Vegfr3*$^{lz/+}$;*p110α*$^{D933A/+}$ animals were recovered at normal Mendelian ratio with no detectable gross abnormalities (Figure S1A). Immunofluorescence analysis using the established lymphatic markers Nrp2 and Prox1 showed that the majority (8 of 10) of double-heterozygous embryos completely lacked mesenteric and intestinal submucosal lymphatic vessels at embryonic day (E)14–E17 (Figures 1A, 1B, and S1D). Mice that do not develop any mesenteric lymphatic vessels are expected to die shortly after birth, as they are unable to absorb dietary fats. In agreement, about 50% of the double-heterozygous mice died immediately after birth (Figure S1A). Mutants with a complete loss of lymphatic vessels were only observed at P0 (data not shown), while from P1 onward, all surviving pups had at least one mesenteric lymphatic vessel (Figure 1B; data not shown). Additionally, the mesenteric lymph sac at the root of the mesentery was reduced in size or absent in the *Vegfr3*$^{lz/+}$;*p110α*$^{D933A/+}$ embryos (Figures 1A and 1C). Surprisingly, however, lymphatic vessels in the diaphragm, which are thought to develop from the same lymph sac as the mesenteric lymphatic vasculature, as well as dermal lymphatic vessels formed in *Vegfr3*$^{lz/+}$;*p110α*$^{D933A/+}$ mice (Figures 1A, 1D, and S1E). Blood vasculature in the skin, mesentery, and intestine also was unaffected in the double-heterozygous mice (Figures 1A, S1C, and S1D). p110α specifically cooperated with VEGFR-3 and not VEGFR-2, the other lymphatic endothelial VEGFR, since *Vegfr2*$^{flox/-}$;*p110α*$^{D933A/+}$ mice developed into adulthood and showed normal lymphatic vasculature (Figures S2A and S2B).

To further explore the selective requirement of VEGFR-3/PI3K signaling for mesenteric lymphatic vessel development, we genetically deleted *p110α* in all lymphatic vessels by crossing *p110α*^{flox} mice (Graupera et al., 2008) with *Vegfr3-CreER*^{T2} animals (I.M.-C. and S.O., unpublished data). To first validate the previously unpublished *Vegfr3-CreER*^{T2} mice, we crossed them to the *R26-mTmG* reporter mice that allow monitoring of Cre activity by the expression of membrane-bound green fluorescent protein (GFP) and concomitant inactivation of red fluorescent protein Tomato expression (Muzumdar et al., 2007). The 4-hydroxytamoxifen (4-OHT) administration to pregnant females led to efficient Cre-mediated recombination in dermal (85.8% ± 2.0%, n = 4) and mesenteric (78.6% ± 7.0%, n = 4)

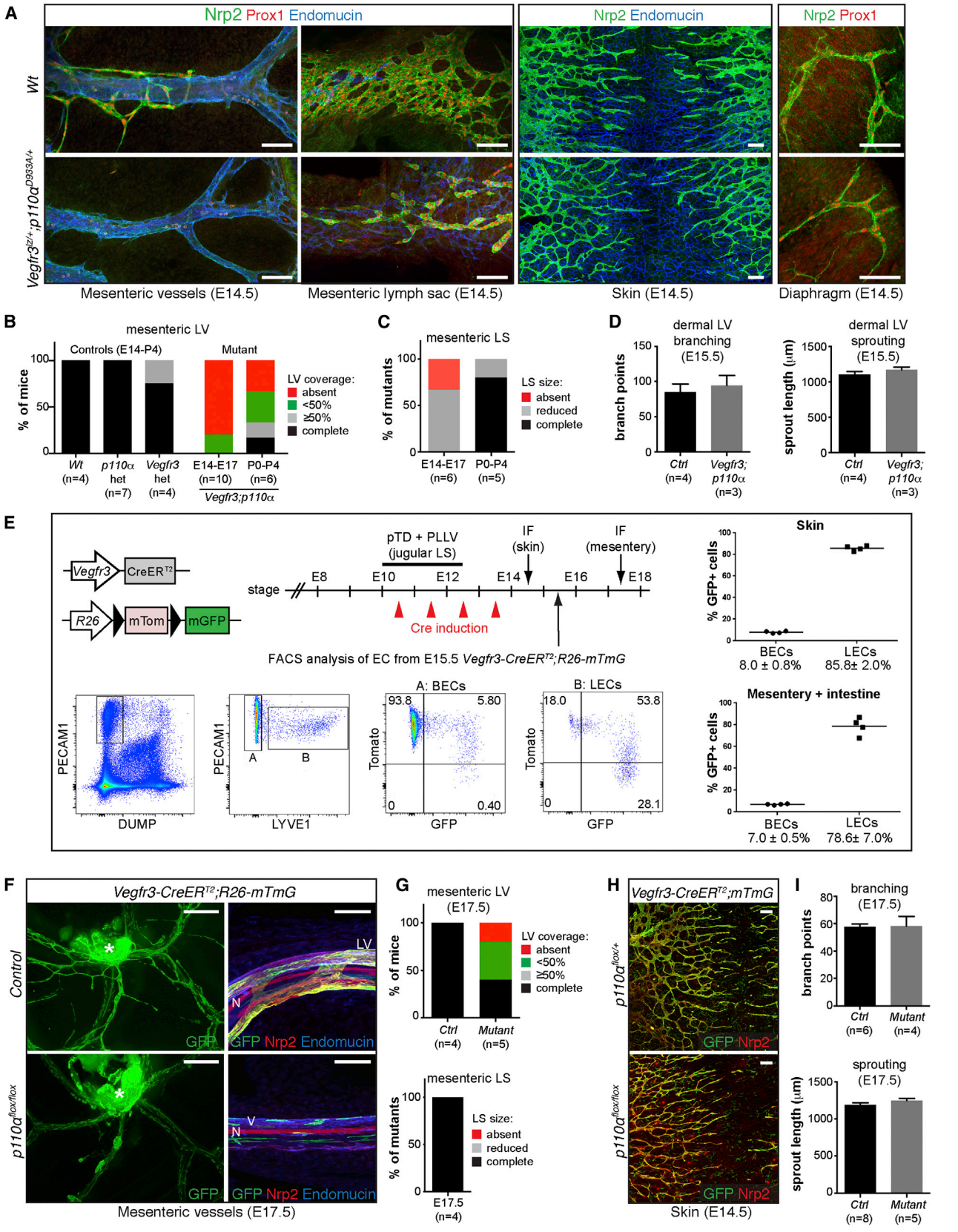

(legend on next page)

lymphatic vessels in *Vegfr3-CreER^{T2};R26-mTmG* embryos at E15.5 (Figures 1E and S3A). On the contrary, Cre recombination in blood endothelia was very low (8.0% ± 0.8% and 7.0% ± 0.5% in skin and mesentery, respectively, n = 4) (Figure 1E). Similar recombination efficiency was observed at E17.5 (Figure S3B). In control mesentery, lymphatic vessels were visualized by GFP fluorescence (Figure 1F). In contrast, deletion of *p110α* in all lymphatic vessels in *p110α$^{flox/flox}$; Vegfr3-CreER^{T2};R26-mTmG* mice led to a reduced number of mesenteric lymphatic vessels, although the mesenteric lymph sac formed normally (Figures 1F and 1G). Dermal lymphatic vessels showed normal sprouting and branching in the mutant compared to control embryos (Figures 1H and 1I). Dermal and mesenteric blood vessels also appeared normal in the mutants (Figure 1F; data not shown), as expected given the low level of Cre-mediated *p110α* deletion in blood endothelia in the *Vegfr3-CreER^{T2}* line (Figure 1E). Together, these results demonstrate a selective requirement of VEGFR-3/PI3K signaling, mediated via the p110α PI3K pathway, for the formation of mesenteric lymphatic vasculature.

Venous-Derived LECs Form the Mesenteric Lymph Sac

Next we investigated whether the mesentery-specific VEGFR-3/PI3K signaling requirement reflects a unique mechanism of vessel formation in this tissue. Early lymphatic development in the jugular region, where LECs were shown to differentiate within cardinal and superficial veins, has been studied extensively (Hägerling et al., 2013; Srinivasan et al., 2007; Yang et al., 2012). Following their exit from the veins, LECs form the peripheral longitudinal lymphatic vessel (PLLV) and primordial thoracic duct (pTD), commonly referred to as jugular lymph sac, from which vessels sprout further to peripheral organs such as skin (Hägerling et al., 2013; Srinivasan et al., 2007; Yang et al., 2012). In the mesentery, LECs are thought to similarly differentiate within major veins at the root of the mesentery and exit the veins to form a single retroperitoneal (also called mesenteric) lymph sac, from which vessels of the mesentery and the diaphragm are formed (Sabin, 1902; van der Putte, 1975; Figure 2A). To capture this process, we analyzed the mesenteric root between E12 and E14 using high-resolution immunofluorescence confocal microscopy. Using Prox1 and Endomucin as markers of LECs and venous blood endothelial cells (BECs), respectively, we first detected Prox1-positive LECs within the superior mesenteric vein at E12.5 (Figure 2B). At E13 all Prox1-positive cells were found outside the vein organized in cord-like structures and expressing high levels of the established LEC marker Nrp2 (Figure 2B). At E14, LECs formed an extensive lymphatic plexus adjacent to the superior mesenteric vein (Figure 2B). These data are consistent with the current model of lymphatic development, and they suggest that the mesenteric lymph sac is of venous origin and forms between E12 and E14.

The origin of the mesenteric lymph sac was analyzed further by lineage tracing using an inducible endothelial-specific *Pdgfb-CreER^{T2}* line (Claxton et al., 2008) in combination with the *R26-mTmG* double reporter (Figure 2C). Upon 4-OHT administration, *Pdgfb*-expressing endothelial cells and their descendants were labeled with GFP. Genetic labeling of blood endothelium by GFP at E11/E12, just prior to the onset of mesenteric lymphatic development, led to significant labeling of the lymph sac (Figure 2C), thus confirming the contribution of venous-derived cells to the mesenteric lymph sac.

Mesenteric Lymphatic Vessels Form via the Assembly of Isolated Endothelial Cell Clusters

We next analyzed the formation of mesenteric lymphatic vessels that run parallel to mesenteric veins (Figure 2A) and are thought to develop by sprouting from the mesenteric lymph sac. Surprisingly, we observed isolated clusters of endothelial cells that were positive for the LEC markers Prox1 and Nrp2 and located along mesenteric veins in the absence of continuous vessel sprouts from the lymph sac (Figure 3A). Clusters appeared between E13 and E13.5, rapidly increased in size and number, and coalesced to form lymphatic vessels by E14.5 (Figure 3A). Different stages of cluster and vessel formation frequently were observed within the same mesentery along different artery-vein pairs, suggesting that cluster formation and coalescence occur during a brief window of time (Figures 3A and S4A).

Figure 1. Organ-Specific Requirement of VEGFR-3/p110α PI3K Signaling for Mesenteric Lymphatic Vessel Development

(A) Whole-mount immunofluorescence of E14.5 wild-type and *Vegfr3$^{lz/+}$;p110α$^{D933A/+}$* tissues for LEC markers Nrp2 (green) and Prox1 (red) and venous EC marker Endomucin (blue). Mutant embryos lack lymphatic vessels (LVs) specifically in the mesentery.

(B and C) Quantification of mesenteric LV (MLV) and lymph sac (MLS) phenotypes in *Vegfr3$^{lz/+}$;p110α$^{D933A/+}$* mice at embryonic (E14–E17) and early postnatal (P0–P4) stages. All controls showed complete LV coverage. In (C), complete represents the size of LS in control littermates (n = 5 [E14–E17] and n = 5 [P0–P4]).

(D) Quantification of dermal LV branching and sprouting in E15.5 wild-type and *Vegfr3$^{lz/+}$;p110α$^{D933A/+}$* embryos, showing no differences between the groups. Data represent mean ± SEM.

(E) (Top) Schematic of the *Vegfr3-CreER^{T2}* transgene, *R26-mTmG* reporter construct, and 4-OHT administration (Cre induction, red arrowheads) schedule. mTom/mGFP, membrane-bound Tomato/GFP. The timing of pTD and PLLV formation is indicated. FACS analysis of endothelial cells from E15.5 *Vegfr3-CreER^{T2};R26-mTmG* embryos showing GFP expression, indicating Cre recombination, in LECs and to a lesser extent in BECs. (Bottom) Representative FACS plots and gating scheme. (Right) Graphs of all results; the horizontal lines represent mean (n = 4).

(F and H) Whole-mount immunofluorescence of control (*p110α$^{flox/+}$* or *p110α$^{+/+}$;Vegfr3-CreER^{T2};R26-mTmG*) and p110α mutant (*p110α$^{flox/flox}$;Vegfr3-CreER^{T2};R26-mTmG*) mesenteries (E17.5) and skin (E14.5) for indicated proteins. 4-OHT (1.5 mg) was administered at E10.5, E11.5, E12.5, and E13.5. GFP shows efficient Cre-mediated recombination in LVs and lack of vessels in the mutant mesentery. A mosaic pattern of recombination is detected in blood vessels. Note that Nrp2 is additionally expressed in the nerves and veins. Asterisk, MLS; N, nerve (Nrp2^{+}); V, vein (Endomucin^{+}).

(G) Quantification of MLV and MLS phenotypes. For LS, complete represents the size of LS in controls (n = 3).

(I) Quantification of dermal LV branching and sprouting in E17.5 control and *p110α$^{flox/flox}$;Vegfr3-CreER^{T2}* embryos, showing no differences between the groups. Data represent mean ± SEM.

See also Figures S1–S3 and Table S1.

Scale bars, 100 μm (A and F; mesenteric vessels, LS, diaphragm), 200 μm (A and H; skin), and 1 mm (mesentery whole-mount).

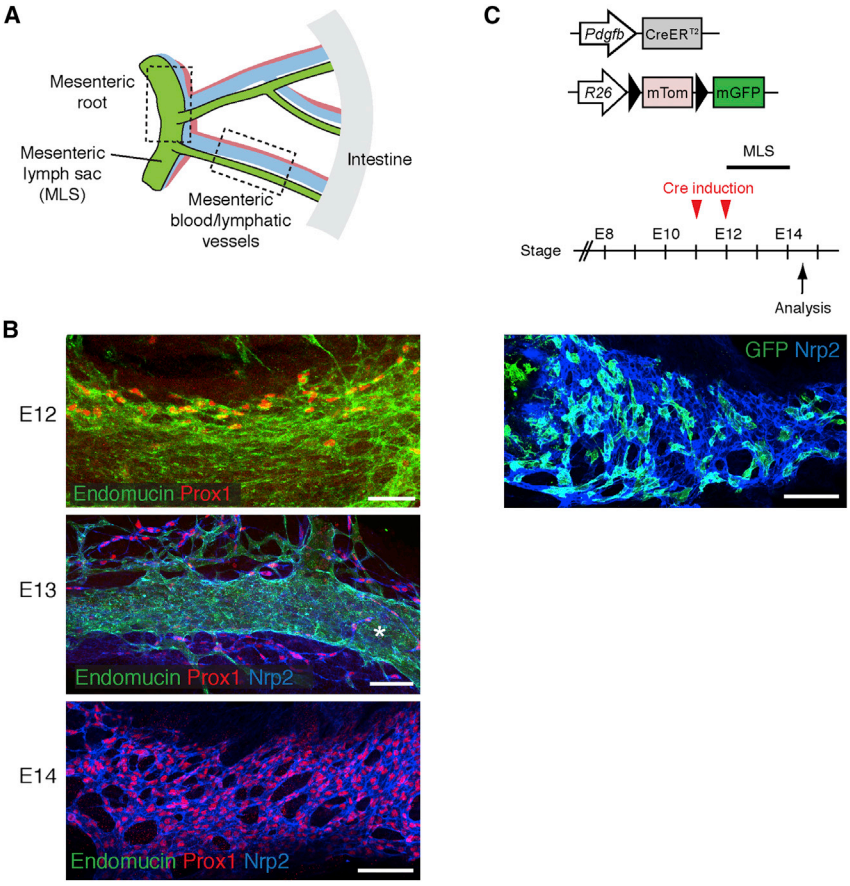

Figure 2. Venous-Derived LECs Form the MLS

(A) Schematic illustration of mesenteric vasculature. Blue, vein; red, artery; green, LV. Boxed regions indicate areas analyzed by immunofluorescence.

(B) Whole-mount immunofluorescence of the developing LS at the root of the mesentery for indicated proteins. Stages of development are shown. At E14 only the LS is visualized. Asterisk, superior mesenteric vein.

(C) Schematic of the inducible *Pdgfb-CreER^{T2}* transgene and *R26-mTmG* reporter construct used for lineage tracing of venous endothelia. The timing of MLS formation is indicated. 4-OHT (1 mg) was administered at E11 and E12 (red arrowheads) and the MLS was analyzed at E14 by immunofluorescence with antibodies against GFP (green) and Nrp2 (blue). LS showing mosaic GFP labeling is shown.

Scale bars, 100 μm.

We reasoned that the isolated LEC clusters could be formed of cells that detached from the lymph sac and migrated along the mesenteric veins. Alternatively, they may have differentiated locally from mesenteric veins. To address these possibilities, we characterized the morphological and molecular features of LEC clusters. Cell shape was first analyzed by labeling individual LECs with membrane-bound GFP using the *Vegfr3-CreER^{T2};R26-mTmG* mice and a suboptimal dose of 4-OHT. Cells within mesenteric LEC clusters extended long membrane protrusions, often in a non-polarized fashion (Figure 3B), and showed rounded nuclear morphology (Figure 3C). This was in contrast to the elongated nuclear morphology that is associated with a migratory phenotype (Kim et al., 2014), and that we observed in LECs upon cluster coalescence into vessels (Figure 3C). Venous-derived LECs forming the mesenteric lymph sac (Figure 3C), as well as the PLLV and pTD (Hägerling et al., 2013), also showed a more elongated nuclear morphology (Figure 3C). Mesenteric LECs within clusters thus lack features typical of polarized cells undergoing directional migration, which argues against their rapid migration from the lymph sac.

Mesenteric LEC clusters expressed the (lymphatic) endothelial markers Prox1, Nrp2, VEGFR-3, VEGFR-2, and Podoplanin (Figure 3D). They were proliferative as indicated by EdU incorporation (Figure 3D). Surprisingly, LEC clusters expressed very low levels of LYVE-1, which was highly expressed in lymph sac endothelium (Figure 3E). In addition, LEC clusters did not express BEC markers CD34 and Endomucin, or hematopoietic markers Sca1, CD41, c-Kit, or CD45 (Figures 3F and S4B). Lack of CD34 and Endomucin expression in mesenteric LECs suggests that they do not arise by local differentiation and budding from veins, which has been reported to lead to perdurance of BEC marker expression for 24 hr (Hägerling et al., 2013).

We sought further evidence for non-venous origin of mesenteric lymphatic vessels by analyzing mice carrying *Cldn5-GFP* transgene that labels all vessels, including mesenteric arteries, veins, and the lymph sac, by strong GFP fluorescence (Figure 3G). If generated in situ from the existing mesenteric vasculature, perdurance of GFP is expected to lead to GFP labeling of LECs, regardless of *Cldn5* promoter activity. However, a major proportion of LECs in E14 *Cldn5-GFP* mesenteries were GFP$^-$ (Figures 3G and 3H). Isolated single Prox1$^+$ LECs and clusters of two cells were mostly GFP$^-$ (Figure 3H). Larger clusters showed variability in GFP expression with some cells expressing high levels of GFP, equivalent to those detected in already formed vessels, while others were GFP$^-$ (Figure 3H). The progressive increase in the intensity of GFP from single cells to larger clusters suggests induction of *Cldn5* expression first upon cluster and vessel formation. Importantly, the abundance of GFP$^-$ LECs suggests that mesenteric lymphatic vessels are not derived from mesenteric blood vessels or the venous-derived lymph sac.

Mesenteric Lymphatic Vessels Originate from Non-venous Endothelium

To trace the cell of origin of mesenteric LECs, we employed temporal lineage tracing using the endothelial-specific *Pdgfb-CreER^{T2}* line in combination with the *R26-mTmG* reporter. We found that when 4-OHT was administered at E8–E8.5, to target blood endothelium prior to the initiation of lymphatic development (Figure 4A), mesenteric arteries and veins showed poor

or no labeling, respectively. Surprisingly, however, traced GFP$^+$ cells were present in the mesenteric LEC clusters and, to a lesser degree, in the lymph sac (Figures 4B and S5A). On the contrary, 4-OHT administration at E9 or later resulted in increased labeling of mesenteric blood vessels but decreased labeling of LECs (Figure S5A). Fluorescence-activated cell sorting (FACS) analysis confirmed an overall increase in the labeling of blood endothelia, as well as venous-derived LECs, in E9 compared to E8 4-OHT-treated embryos (Figure S5B). Taken together, these results suggest selective targeting of LEC progenitors in the mesentery upon early induction of *Pdgfb-CreER^{T2}*. Furthermore, efficiency of LEC labeling upon Cre induction at E8–E8.5 varied among different embryos, suggesting a narrow window of time during which the cell of origin of mesenteric LECs can be targeted and/or when LEC progenitors are generated (Figure S5A).

To identify the source of mesenteric LECs, we carried out detailed characterization of Cre recombination pattern in *Pdgfb-CreER^{T2};R26-mTmG* embryos that were treated with 4-OHT at E8–E8.5. Whole-mount immunofluorescence of E9.5 embryos showed only a few scattered GFP$^+$ cells in the cardinal and vitelline veins (Figures 4C and S6A). Quantitative FACS analysis of LYVE-1$^+$ LECs, at time points when venous LEC progenitors exit cardinal veins (E10.25) and form the first lymphatic structures pTD and PLLV (E11), showed low levels of recombination (Figure 4D). Immunofluorescence analysis confirmed that venous-derived jugular lymph sacs (pTD and PLLV) were not targeted (Figure S6B). Instead, we observed efficient labeling of major arteries, including the dorsal aorta and vitelline artery (Figures 4C and S6A). Hematopoietic cells including macrophages were also efficiently labeled (Figures 4B and S6C), suggesting the targeting of blood-forming hemogenic endothelium. FACS analysis indeed confirmed targeting of cKit$^+$ hemogenic endothelium in the yolk sac (Figure S6D). Consistent with immunofluorescence data showing efficient targeting of the dorsal aorta and vitelline artery, the major intra- and extraembryonic hemogenic vessels, FACS analysis at E11 revealed that a major population of *Pdgfb-CreER^{T2}*-traced cells in the embryo proper expressed cKit protein (Figure S6D). Together, these results suggest that arterial or hemogenic endothelium can generate mesenteric LEC progenitors.

cKit Lineage Progenitors of Hemogenic Endothelial Origin Contribute to Mesenteric Lymphatic Vessels

To specifically test the involvement of hemogenic endothelium-derived progenitors in lymphatic development, we used the inducible *cKit-CreER^{T2}* mice (Klein et al., 2013). Despite the expression of cKit in hemogenic endothelium (Marcelo et al., 2013; Figure S7A), the *cKit-CreER^{T2}* line did not label efficiently yolk sac vasculature that contains hemogenic endothelium between E7.5 and E9.5, and only rare hematopoietic cells could be traced (Figure S7B). However, 4-OHT administration to pregnant females at E10 (data not shown) or E11 (Figures 5A and 5B) resulted in the presence of traced GFP$^+$ cells in mesenteric LEC clusters in E13.5 *cKit-CreER^{T2};R26-mTmG* embryos. Only a proportion of embryos (5 of 17, 29%) showed GFP$^+$ LECs, most likely due to a low, although highly specific, recombination in cKit$^+$ cells (Figure 5A). Lineage tracing using *Vav-Cre* (de Boer et al., 2003) showed that definitive hematopoietic cells did not, however, contribute to mesenteric lymphatic vessel development (Figure 5C). These data demonstrate the *cKit* lineage hemogenic endothelium-derived progenitors, but not definitive hematopoietic cells, as the source of mesenteric LECs.

Mesenteric Lymphatic Vessel Formation Selectively Requires *Pdgfrb* Lineage Cells

Yolk sac hemogenic endothelium recently was shown to generate, during a narrow window of time between E8.5 and E9.5, cells that colonize the embryo mesenchyme and express mesenchymal markers including PDGFRβ (Azzoni et al., 2014). Interestingly, we found that *Pdgfrb-Cre* transgene (Foo et al., 2006) labeled a significant proportion (38.9% ± 4.7%, n = 24) of Prox1$^+$ cells within mesenteric LEC clusters (Figure 6A). FACS analysis of LECs from E13.5 *Pdgfrb-Cre;R26-mTmG* mesenteries revealed a similar recombination efficiency, but with high inter-individual variation (Figure 6B). As expected, *Pdgfrb-Cre*-mediated recombination was not, however, restricted to LECs. Consistent with the reported expression of PDGFRβ (Foo et al., 2006), recombination also was observed in a large population of mesenchymal and perivascular cells (Figure 6A; data not shown). In addition, we observed low levels of recombination in BECs in multiple tissues (data not shown).

To provide evidence for the functional importance of the *Pdgfrb*-expressing cells for mesenteric lymphatic vessel development, we deleted *Vegfr3*, the key regulator of lymphangiogenesis, in these cells by crossing *Pdgfrb-Cre;R26-mTmG* mice with *Vegfr3^{flox}* animals (Haiko et al., 2008). Analysis of mesenteries between E15.5 and E18.5 revealed the absence of lymphatic vessels in 44% of the *Vegfr3$^{flox/flox}$;Pdgfrb-Cre* embryos (n = 16) (Figures 6C and 6D). Similar to the *Vegfr3$^{lz/+}$;p110α$^{D933A/+}$* embryos, mesenteric lymph sac also was reduced in size or absent in the majority of those *Vegfr3$^{flox/flox}$;Pdgfrb-Cre* embryos that showed lymphatic defects (Figure 6E). However, lymphatic vessels of the thoracic skin formed in all (12 of 12) *Vegfr3$^{flox/flox}$;Pdgfrb-Cre* embryos analyzed (Figure 6C; data not shown). These results demonstrate a selective requirement of *Pdgfrb*-expressing LEC progenitor cells for mesenteric lymphatic vessel development, and they provide functional evidence for organ-specific mechanisms of vessel formation.

In conclusion, our results demonstrate organ-specific mechanisms of lymphangiogenesis and origin of the vasculature. Contrary to current dogma that veins are the sole origin of the entire lymphatic vasculature in mammals (Srinivasan et al., 2007), we show that part of the mesenteric lymphatic vasculature is derived from *cKit* lineage progenitor cells of hemogenic endothelial origin (Figure 7). Our data further indicate that these progenitors give rise to LECs in the mesentery through a lymphvasculogenic process that is critically dependent on VEGFR-3/PI3K signaling.

DISCUSSION

Human vascular diseases are often restricted to specific vessel types or vascular beds of specific organs, but what underlies tissue-specific vessel failure is poorly understood. In this study we uncover an organ-specific role for VEGFR-3/PI3K signaling in mesenteric lymphatic vessel formation. We further identify

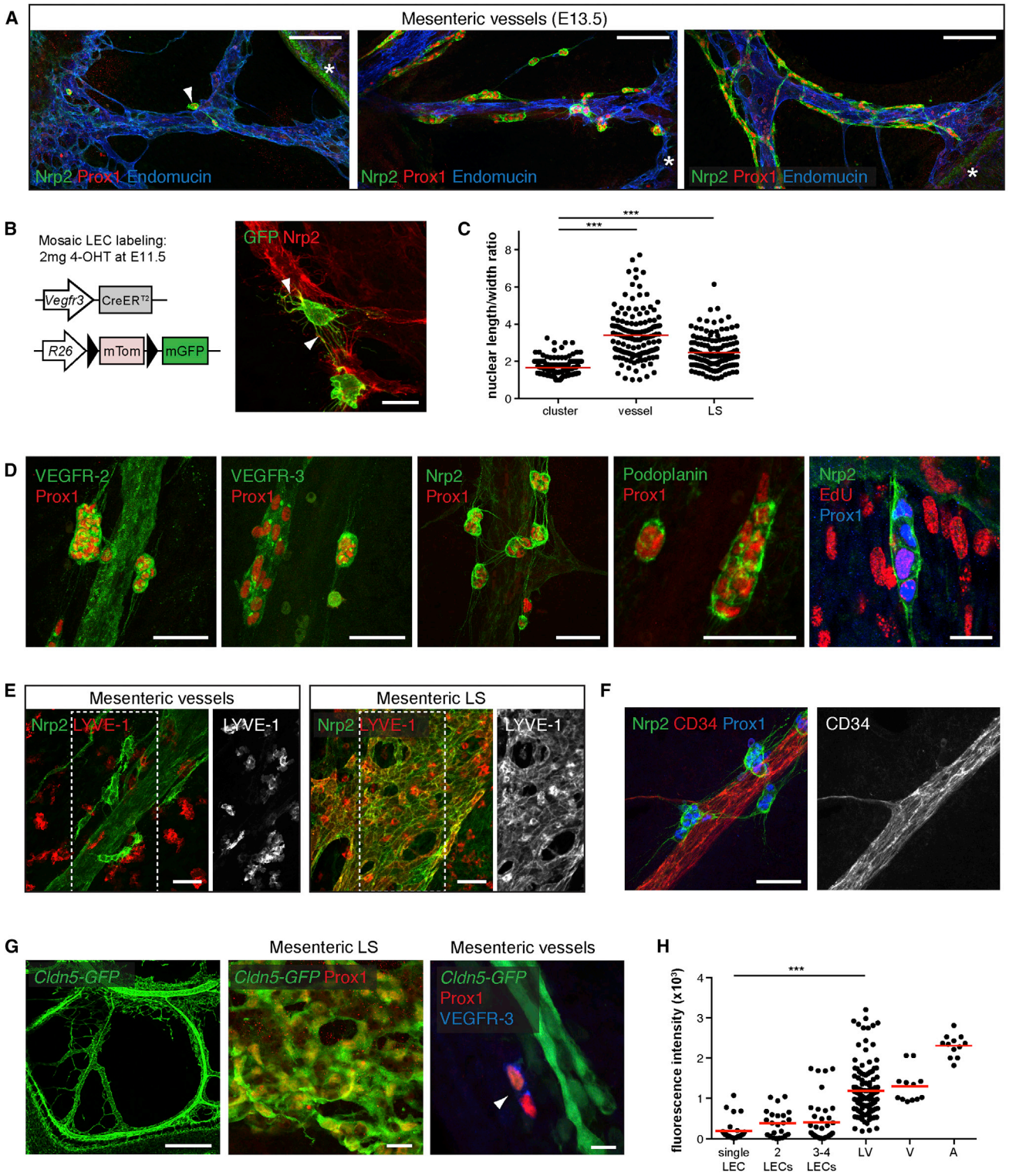

Figure 3. MLVs Form via the Assembly of Isolated LEC Clusters

(A) Whole-mount immunofluorescence of the developing MLVs from three embryos harvested at E13.5 for indicated proteins, showing different stages of LEC cluster formation and coalescence. Note the presence of isolated LEC clusters (arrowhead) in the absence of sprouts from the MLS. Asterisks, intestinal wall. (B) Analysis of LEC cell shape with membrane-bound GFP in E13.5 *Vegfr3-CreER^{T2};R26-mTmG* vessels. 4-OHT (2 mg) was administered at E11.5 to induce mosaic LEC labeling. Arrowheads point to non-polarized filopodia.

(legend continued on next page)

hemogenic endothelium as a previously unknown tissue of origin for lymphatic vessels in the mesentery. Our results suggest that heterogeneity in endothelial origin may contribute to tissue-specific formation and functional specialization of vessels during development and vessel failure in disease.

VEGFR-3 is the key regulator of lymphangiogenesis, controlling lymphatic endothelial cell proliferation, migration, and survival. Inhibition of VEGFR-3 signaling in the mouse skin using a soluble ligand trap led to lymphatic vessel hypoplasia, while genetic deletion of its ligand, *Vegfc*, resulted in a complete absence of lymphatic vasculature due to failure of vessel sprouting from the veins (Hägerling et al., 2013; Karkkainen et al., 2004; Mäkinen et al., 2001a). As expected from these results, homozygous deletion of *Vegfr3* resulted in severe lymphatic vessel hypoplasia in multiple tissues, including the skin and mesentery (L.S. and T.M., unpublished data and this study). The VEGFR-3 downstream signaling events controlling the different endothelial cell responses during vascular morphogenesis remain unclear, but in vitro studies have shown that VEGFR-3 activates the Ras/MAPK and PI3K/Akt pathways (Coso et al., 2012; Lapinski et al., 2012; Mäkinen et al., 2001b).

PI3K signaling, particularly through its catalytic subunit p110α, has emerged as a key regulator of vascular development (Graupera and Potente, 2013). p110α is critically required for endothelial cell migration downstream of VEGFR-2 during angiogenesis (Graupera et al., 2008), while its aberrant activation has been implicated in the development of blood and lymphatic vascular malformations in human syndromes (Brouillard et al., 2014). In this study we identified a strong genetic interaction between *p110α* and *Vegfr3* during mesenteric and intestinal, but not dermal lymphatic development, suggesting a cooperative function of these genes selectively in the mesentery. In agreement with this observation, lymphatic endothelial-specific full deletion of *p110α* resulted in a selective failure of mesenteric lymphatic vessel formation. Contrary to its role in controlling BEC migration upon VEGF/VEGFR-2 activation, *p110α* deficiency did not impair lymphatic vessel sprouting in embryonic skin. These data suggest that p110α regulates different functions downstream of VEGFR-2 and VEGFR-3 in BECs and LECs, respectively. The organ-specific role of p110α further indicates that, in tissues other than the mesentery, VEGFR-3 signaling does not depend on p110α. Previous studies have shown the requirement of the PI3K regulatory subunits p85/p55/p50α and the interaction of Ras with p110α in the development and remodeling of multiple lymphatic vascular beds (Gupta et al., 2007; Mouta-Bellum et al., 2009). It is therefore possible that p110α function is compensated by the p110β and/or p110δ subunits in lymphatic vascular beds other than the mesentery.

The origin of the lymphatic vasculature has been debated for over a century. Florence Sabin described in the early 20th century that lymphatic vessels are derived from embryonic veins (Sabin, 1902). Recent molecular biological data not only support the concept of transdifferentiation of venous into LECs, but also suggest that they are the sole origin of the entire lymphatic vasculature in mammals (Oliver and Srinivasan, 2010; Srinivasan et al., 2007). Other contributing sources of LECs have been suggested though never demonstrated to contribute to mammalian lymphatic vasculature. In the early 1900s, Huntington and McClure proposed that LECs derive from mesenchymal precursors (Huntington and McClure, 1910). Based on expression analyses, such precursor cells were described in *Xenopus* (Ny et al., 2005), chicken (Wilting et al., 2000), and mouse (Buttler et al., 2006), although no functional validation has been provided. Grafting experiments further suggested that avian lymphatic vasculature is of dual origin, with a contribution from both venous- and mesenchymal-derived cells (Wilting et al., 2006). In addition, hematopoietic cell-derived endothelial progenitors and transdifferentiating leukocytes and macrophages were shown to participate in pathological lymphangiogenesis (Kerjaschki et al., 2006; Maruyama et al., 2005; Salven et al., 2003). The identity of these additional sources of LECs and their requirement for lymphatic vascular morphogenesis, however, was questioned by findings that demonstrated the venous origin of LECs (Oliver and Srinivasan, 2010; Srinivasan et al., 2007), and excluded macrophages as a source of lymphatic endothelia (Gordon et al., 2010). In this study we identified *cKit* lineage hemogenic endothelial cells as a novel, organ-specific origin of mesenteric lymphatic vessels. Mesenteric lymph sac instead forms from venous-derived LECs, with a minor contribution from the hemogenic endothelium-derived progenitors.

Similar to the two processes of blood vessel formation, vasculogenesis, and angiogenesis, the mechanisms of mesenteric lymph sac and vessel formation are fundamentally different. Blood vessel formation is initiated in the developing embryo via differentiation and assembly of mesodermal precursor cells (vasculogenesis), after which most if not all blood vessel formation occurs via sprouting from pre-existing vasculature (angiogenesis). We found that mesenteric lymphatic vascular development occurs in a fundamentally different manner. It is initiated at E12.5 via formation of the mesenteric lymph sac through an angiogenic process that involves LEC differentiation within and sprouting from the veins. The mesenteric lymphatic vessels are formed subsequently via differentiation and assembly of lymphatic endothelial progenitors of hemogenic endothelial origin into cell clusters and vessels through a process resembling vasculogenesis, which we thus defined as lymphvasculogenesis. During

(C) Quantification of nuclear morphology of LECs in clusters (n = 135 cells), vessels (n = 141 cells), and developing LS (n = 123 cells) at E13.5. The horizontal lines represent mean values. ***$p < 0.0001$.

(D–F) Whole-mount immunofluorescence of isolated LEC clusters and MLS for indicated proteins. Single-channel images are shown for the boxed regions in (E and F) for indicated stainings.

(G) Whole-mount immunofluorescence of E14 *Cldn5-GFP* mesenteries for indicated proteins. Note GFP^- LEC cluster (arrowhead) but strong GFP expression in blood vessel and LS endothelia.

(H) Quantification of GFP fluorescence intensity in endothelial cells in E14 *Cldn5-GFP* mesenteries. For LECs, single cells and clusters of two and three to four cells are shown. V, vein; A, artery. The horizontal lines represent mean values. ***$p < 0.0001$.

See also Figure S4.

Scale bars, 100 μm (A), 20 μm (B and G, right), 50 μm (D–F), and 500 μm (G, left).

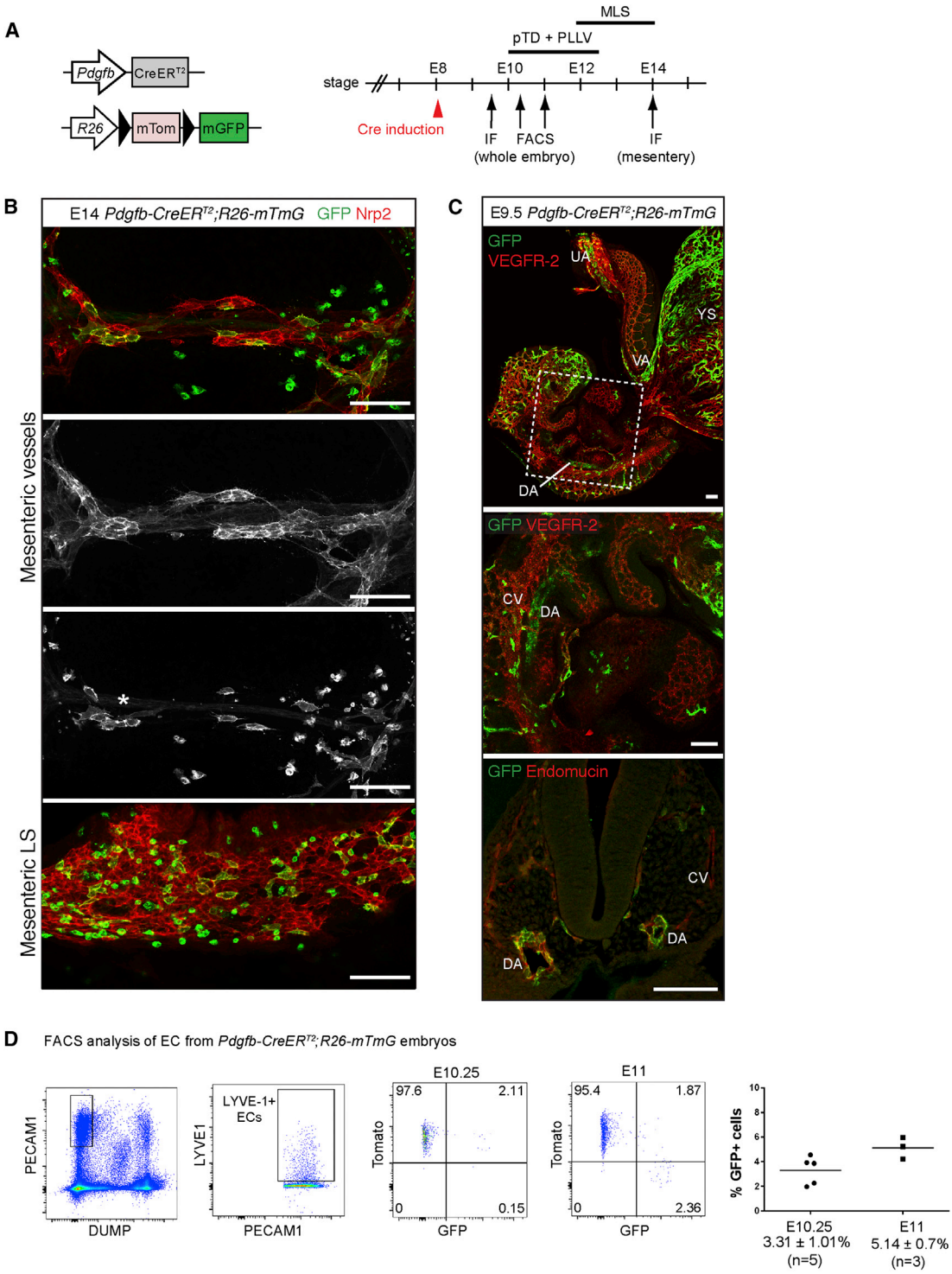

Figure 4. MLVs Originate from Non-venous Endothelium

(A) Schematic of the *Cre* transgene, *R26-mTmG* reporter construct, and 4-OHT administration protocol (red arrowhead, 2 mg) used for lineage tracing.

(B) Tile scans of E14 *Pdgfb-CreER^{T2};R26-mTmG* mesenteries stained with antibodies against GFP (green) and Nrp2 (red). Single-channel images are shown. Note weak GFP staining (asterisk) in the artery from the *ires-GFP* cassette within the *Pdgfb-CreER^{T2}* transgene.

(C) Immunofluorescence staining of E9.5 *Pdgfb-CreER^{T2};R26-mTmG* whole embryo (top) and transverse vibratome section (bottom) for indicated proteins. Note efficient Cre-mediated recombination (green) in dorsal aorta (DA), vitelline (VA), and umbilical artery (UA), and yolk sac (YS) vasculature, but not in cardinal vein (CV). Boxed area is magnified in the middle.

(legend continued on next page)

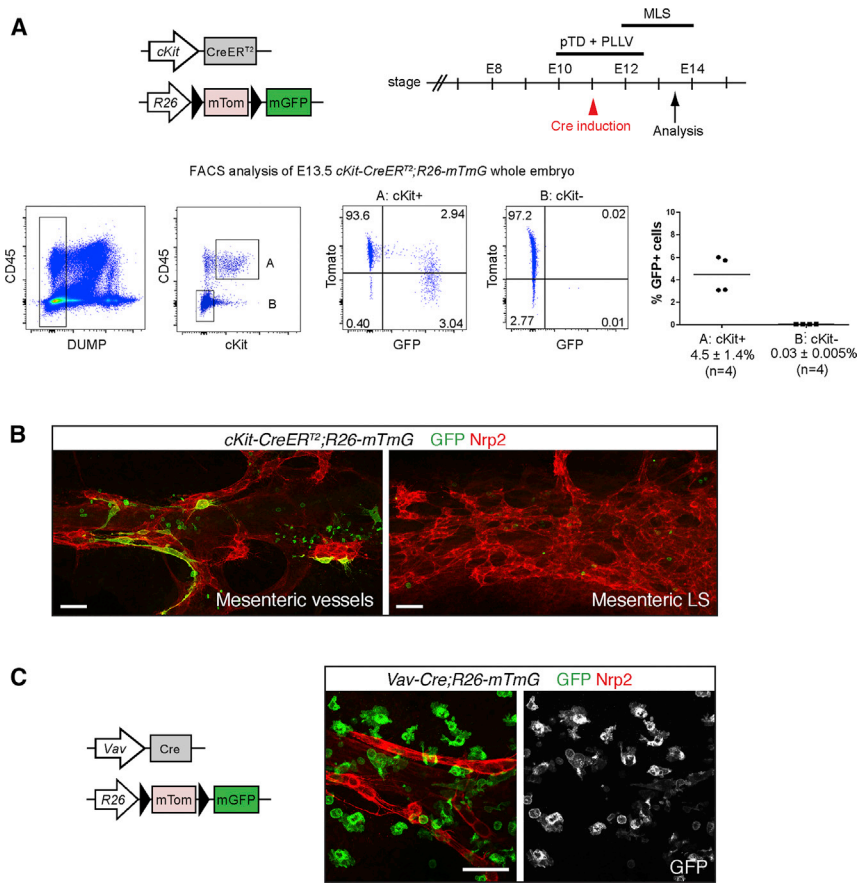

Figure 5. MLVs Derive from *cKit* Lineage Cells of Hemogenic Endothelial Origin

(A) (Top) Schematic of the *Cre* transgene, *R26-mTmG* reporter construct, and 4-OHT administration protocol (red arrowhead, 2 mg) used for lineage tracing. (Bottom) FACS analysis of endothelial cells from E13.5 *cKit-CreER^{T2};R26-mTmG* embryos showing specific but inefficient Cre-mediated recombination in cKit$^+$ cells. Representative FACS plots and gating scheme and graph of all results are shown. The horizontal lines represent mean (n = 4).

(B) Tile scans of E13.5 *cKit-CreER^{T2};R26-mTmG* mesenteries stained with antibodies against GFP (green) and Nrp2 (red).

(C) Schematic of the *Vav-Cre* transgene and *R26-mTmG* reporter construct, and whole-mount immunofluorescence of mesenteric vessels from E14.5 *Vav-Cre;R26-mTmG* embryo for GFP (green) and Nrp2 (red). Single-channel image for GFP is shown. See also Figure S7.

Scale bars, 50 μm.

this process, mesenteric LECs extend long filopodia that interconnect cells from different clusters. These often non-polarized filopodia may play a role in cell-cell communication during cluster coalescence, similar to the role of blood endothelial filopodia in vessel anastamosis (Lenard et al., 2013; Phng et al., 2013).

Hemogenic endothelium is a de novo source of transient definitive hematopoietic progenitors during a narrow developmental window between E7.5 and E11 of mouse development, before first liver and then bone marrow become the main hematopoietic organs. Hemogenic endothelium is found at specific anatomical sites, including the yolk sac, placenta, vitelline artery, and the AGM region that contains the dorsal aorta (Hirschi, 2012). Recently, a subset of endocardial cells in the outflow cushion and atria of the heart also was shown to possess hemogenic activity, suggesting the existence of organ-specific sites of embryonic hematopoiesis (Nakano et al., 2013). Interestingly, the progeny of hemogenic endothelial cells may be functionally different depending on their site of origin (Hirschi, 2012). It therefore will be important to define the specific anatomic site(s) that gives rise to mesenteric LEC progenitors. However, due to a limitation of tools for tracing cells of hemogenic endothelial origin at different developmental stages, it was not possible to define the timing and contribution of different hemogenic sites to the generation of mesenteric LECs in this study. 4-OHT induction of *cKit-CreER^{T2}* at E10 or E11 did not allow us to distinguish if the source of mesenteric LECs are cKit$^+$ progenitors, derived either from extra- or intraembryonic hemogenic endothelium, or cKit$^+$ hemogenic endothelium in the embryo proper (including AGM), which are all present at E10–E11. Unveiling how the hemogenic endothelial-derived progenitors reach the mesenteries is also an interesting question for further research. One possibility is that they arrive via circulation, which is followed by their extravasation and differentiation into LECs. Alternatively, these cells may migrate directly from the site of emergence to the mesentery. In support of the latter possibility, it has been shown that primitive myeloid progenitors that arise in the yolk sac before E8 migrate to the cephalic region of the embryo before the onset of blood circulation and develop into microglia (Alliot et al., 1999; Ginhoux et al., 2010).

It has been suggested that differences in embryonic origins of vascular smooth muscle cells can contribute to tissue-specific localization of vascular diseases, such as aortic aneurysm and vascular calcification (Sinha et al., 2014). It is similarly plausible that organ-specific manifestation of lymphatic vessel dysfunction in disease is due to vascular bed-specific differences in their

(D) FACS analysis of endothelial cells from E10.25 and E11 *Pdgfb-CreER^{T2};R26-mTmG* embryos showing low Cre-mediated recombination efficiency in venous-derived LECs. Representative FACS plots and gating scheme (shown for E10.25) and graph of all results are shown. The horizontal lines represent mean (n = 5 [E10.25] or n = 3 [E11]).

See also Figures S5 and S6.

Scale bars, 100 μm.

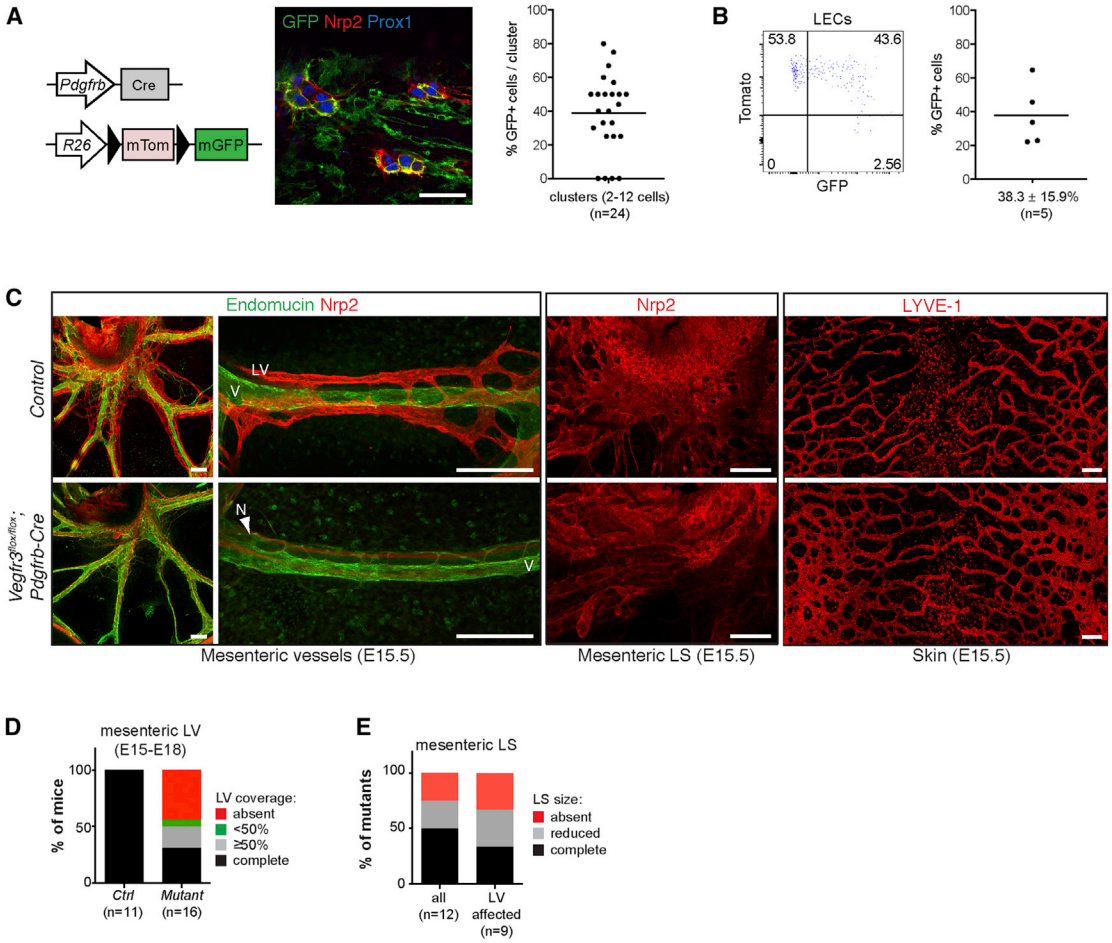

Figure 6. *Vegfr3* Deletion Using the *Pdgfrb-Cre* Leads to Organ-Specific Defect in MLV Formation

(A) (Left) Schematic of the *Pdgfrb-Cre* transgene and *R26-mTmG* reporter construct. (Middle) Whole-mount immunofluorescence of mesenteric LEC clusters in *Pdgfrb-Cre*;*R26-mTmG* mesentery. (Right) Quantification of GFP$^+$ LECs within mesenteric clusters. The horizontal line represents mean (n = 24).

(B) FACS analysis of LECs from E13.5 *Pdgfrb-Cre*;*R26-mTmG* embryos showing variable Cre-mediated recombination. Representative FACS plot and graph of all results are shown. The horizontal line represents mean (n = 5).

(C) Whole-mount immunofluorescence of E15.5 control and *Vegfr3*$^{flox/flox}$;*Pdgfrb-Cre* mesenteries and upper thoracic skin for indicated proteins, showing organ-specific defect in MLV formation in the mutant. LV, lymphatic vessel (Nrp2$^+$); V, vein (Endomucin$^+$); N, nerve (Nrp2$^+$).

(D and E) Quantification of MLV and MLS phenotypes in *Vegfr3*$^{flox/flox}$;*Pdgfrb-Cre* embryos. Complete in (E) represents the size of LS in control littermates (n = 6). Scale bars, 50 μm (A) and 200 μm (C).

origin and formation. It is interesting to note that several primary lymphedemas affect vessels of specific tissues. For example, in Milroy disease, caused by kinase-inactivating mutations in the VEGFR-3 gene, lymphedema is restricted to the lower limbs while lymphatic function in the forearms is unimpaired (Mellor et al., 2010).

In summary, we show that part of the mesenteric lymphatic vasculature forms from *cKit* lineage progenitor cells of hemogenic endothelial origin, and not solely from the venous-derived lymph sac as previously thought. We additionally show that molecular mechanisms regulating the development of lymphatic vessels from venous- and non-venous-derived progenitors are different. These findings reveal a hitherto unrecognized organ-specific mechanism of lymphatic vascular morphogenesis, and they raise the possibility that heterogeneity in the cell of origin contributes to tissue-specific vascular properties and disease. In addition, our study identifies a progenitor cell population with potential for therapeutic exploitation to induce lymphatic regeneration following cancer surgery, lymphedema, or tissue trauma. Given the emerging roles of lymphatic vessels in inflammation, immunity, and lipid metabolism, lymphatic endothelial progenitors additionally may provide a novel strategy to treat common diseases associated with lymphatic dysfunction.

EXPERIMENTAL PROCEDURES

Mice

Description of mouse strains is provided in the Supplemental Experimental Procedures. Staging of E9 and E10 embryos was done by counting somite

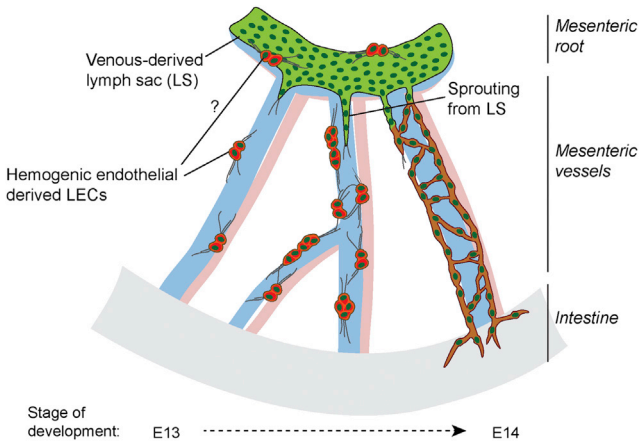

Figure 7. Two Origins of the Mesenteric Lymphatic Vasculature

Schematic model of mesenteric lymphatic vascular development. Venous-derived LECs form the retroperitoneal (M)LS at the root of the mesentery. MLVs instead form by differentiation of *cKit* lineage progenitors of hemogenic endothelial origin. Blue, venous EC; light red, arterial EC; green, LEC; and dark red, non-venous LEC progenitors.

pairs. Embryos harvested before 10 a.m. were typically of stages E0.0–E0.25. For staging of embryos older than E11, the morning of vaginal plug detection was thus considered as E0. For induction of Cre recombination, 4-OHT dissolved in peanut oil (10 mg/ml) was administered to pregnant females by intraperitoneal injections as indicated in figures and/or legends. All mice were maintained on a C57BL/6J genetic background. Experimental procedures were approved by the United Kingdom Home Office and the Uppsala Laboratory Animal Ethical Committee.

Immunofluorescence

For whole-mount immunofluorescence, tissues were fixed in 4% paraformaldehyde (PFA) for 2 hr at room temperature. The samples were washed in PBS, permeabilized in 0.3%-Triton X-100 in PBS (PBSTx) or 1% Triton for E9.5 embryos, and blocked in PBSTx with 3% milk. This was followed by incubation with primary antibodies at 4C overnight in blocking buffer, washing in PBSTx, and incubation with fluorochrome-conjugated secondary antibodies in blocking buffer for 2 hr at room temperature. The tissues were washed and mounted in Mowiol. For E9.5 whole-mount staining, primary and secondary antibodies were incubated for 24 hr each, followed by 8 hr washing in PBST. Details of antibodies are provided in the Supplemental Experimental Procedures.

Flow Cytometry

Embryonic back skin, mesenteries, whole embryos, and yolk sacs were harvested and the tissues were cut into smaller pieces for digestion using a mixture of 1–5 mg/ml Collagenase IV (Life Technologies) and 0.2 mg/ml DNase (Roche) in PBS with 2%–10% fetal bovine serum (FBS) at 37°C under constant rotation for 8–20 min, depending on the tissue. Digests were quenched by adding 2 mM EDTA and filtered through a 70-μm nylon filter (BD Biosciences). Cells were washed with FACS buffer (PBS, 0.5% FBS, and 2 mM EDTA) and immediately processed for staining in 96-well plates. Fc receptor binding was blocked by rat-anti-mouse CD16/CD32 (eBioscience) in all experiments. Details of antibodies are provided in the Supplemental Experimental Procedures. For compensation, the AbC anti-rat/hamster compensation bead kit (Life Technologies) was used. The cells were analyzed on a FACSaria cell sorter utilizing the FACSDiva software (BD Biosciences). Data were processed using FlowJo software (Tree Star). Single cells were gated using FSC-H/FSC-W and SSC-H/SSC-W. FMO controls were used to set up the subsequent gating schemes. All data are presented using biexponential display.

Image Acquisition and Quantification

All confocal images except Figure 5A represent maximum intensity projections of z stacks of single-tile or multiple-tile scan images (see Table S1 for details). Images were acquired using Zeiss 700, 710, or 780 confocal microscopes and Zen 2009-2011 software. Stereomicroscopic images of tissues were acquired with a Leica MZ16F fluorescence microscope equipped with Leica DFC420C camera and Leica Microsystems software. Details about quantification are provided in the Supplemental Experimental Procedures.

Statistical Analysis

GraphPad Prism version 6.0f software was used for graphic representation and statistical analysis of the data. Unpaired t test was applied and results considered statistically significant when $p < 0.05$. Comparisons among multiple groups in Figures 3C and 3G were done by one-way ANOVA (Tukey's multiple comparison test).

SUPPLEMENTAL INFORMATION

Supplemental Information includes Supplemental Experimental Procedures, seven figures, and one table and can be found with this article online at http://dx.doi.org/10.1016/j.celrep.2015.02.026.

AUTHOR CONTRIBUTIONS

L.S. designed the research, performed experiments, interpreted results, and wrote the paper. I.M.-C., M.U., and Y.Z. designed the research, performed experiments, and interpreted results. B.L. and C.B. provided *Cldn5-GFP* mice. M.F. provided *Pdgfb-CreER*^{T2} mice. D.S. provided *cKit-CreER*^{T2} mice. R.H.A. provided *Pdgfrb-Cre* mice. S.O. provided *Vegfr3-CreER*^{T2} mice. K.A. provided *Vegfr3*^{flox} and *Vegfr3*^{lz} mice. M.G. provided *p110α*^{flox} and *p110α*^{D933A} mice. T.M. designed and directed the research, interpreted results, and wrote the paper.

ACKNOWLEDGMENTS

We thank Bart Vanhaesebroeck (UCL Cancer Institute, London) for *p110α*^{flox} and *p110α*^{D933A} mice, Dimitris Kioussis (National Institute for Medical Research, London) for *Vav-Cre* mice, Erwin Wagner for *Vegfr2*^{flox} mice, Ian Roswell and the transgenic services at the LRI for help with establishing mouse lines, Henrik Ortsäter for assistance with experiments, and staff at the LRI and Uppsala University animal units for animal husbandry. We also thank the light microscopy unit at the LRI and BioVis at Uppsala University for advice and help with experiments. This study was supported by Cancer Research UK (L.S., I.M.-C., and T.M.); EMBO Young Investigator Programme, the Kjell and Märta Beijer Foundation, and the Swedish Research Council (T.M.); Fundación Alfonso Martin Escudero (I.M.-C.); Spanish Ministry of Education (FECYT grant, postdoctoral mobility contract EDU/2934/2009; B.L.); MRC G0501711 (M.F.); Deutsche Forschunsgemeinschaft (DFG SA 137/1-3; D.S.); Ministry of Science and Innovation of Spain (grants BIO2009-09488 and SAF2010-18765 to S.O. and grant SAF2010-15661 to M.G.); European Research Council (ERC-2010-AdG-268804 to K.A. and ERC-2011-AdG-294556 to C.B.); Knut and Alice Wallenberg Foundation and the Swedish Cancer Foundation (C.B.); the Leducq Foundation (11CVD03) (K.A.); and the Marie Curie ITN (Vessel, FP7-PEOPLE-2012-ITN; K.A., R.H.A., C.B., and M.G.).

Received: July 3, 2014
Revised: December 29, 2014
Accepted: February 5, 2015
Published: March 12, 2015

REFERENCES

Aird, W.C. (2007a). Phenotypic heterogeneity of the endothelium: I. Structure, function, and mechanisms. Circ. Res. *100*, 158–173.

Aird, W.C. (2007b). Phenotypic heterogeneity of the endothelium: II. Representative vascular beds. Circ. Res. *100*, 174–190.

Alitalo, K. (2011). The lymphatic vasculature in disease. Nat. Med. *17*, 1371–1380.

Alliot, F., Godin, I., and Pessac, B. (1999). Microglia derive from progenitors, originating from the yolk sac, and which proliferate in the brain. Brain Res. Dev. Brain Res. *117*, 145–152.

Armulik, A., Genové, G., Mäe, M., Nisancioglu, M.H., Wallgard, E., Niaudet, C., He, L., Norlin, J., Lindblom, P., Strittmatter, K., et al. (2010). Pericytes regulate the blood-brain barrier. Nature *468*, 557–561.

Azzoni, E., Conti, V., Campana, L., Dellavalle, A., Adams, R.H., Cossu, G., and Brunelli, S. (2014). Hemogenic endothelium generates mesoangioblasts that contribute to several mesodermal lineages in vivo. Development *141*, 1821–1834.

Ben-Zvi, A., Lacoste, B., Kur, E., Andreone, B.J., Mayshar, Y., Yan, H., and Gu, C. (2014). Mfsd2a is critical for the formation and function of the blood-brain barrier. Nature *509*, 507–511.

Brouillard, P., Boon, L., and Vikkula, M. (2014). Genetics of lymphatic anomalies. J. Clin. Invest. *124*, 898–904.

Butler, J.M., Kobayashi, H., and Rafii, S. (2010a). Instructive role of the vascular niche in promoting tumour growth and tissue repair by angiocrine factors. Nat. Rev. Cancer *10*, 138–146.

Butler, J.M., Nolan, D.J., Vertes, E.L., Varnum-Finney, B., Kobayashi, H., Hooper, A.T., Seandel, M., Shido, K., White, I.A., Kobayashi, M., et al. (2010b). Endothelial cells are essential for the self-renewal and repopulation of Notch-dependent hematopoietic stem cells. Cell Stem Cell *6*, 251–264.

Buttler, K., Kreysing, A., von Kaisenberg, C.S., Schweigerer, L., Gale, N., Papoutsi, M., and Wilting, J. (2006). Mesenchymal cells with leukocyte and lymphendothelial characteristics in murine embryos. Dev. Dyn. *235*, 1554–1562.

Claxton, S., Kostourou, V., Jadeja, S., Chambon, P., Hodivala-Dilke, K., and Fruttiger, M. (2008). Efficient, inducible Cre-recombinase activation in vascular endothelium. Genesis *46*, 74–80.

Connell, F.C., Gordon, K., Brice, G., Keeley, V., Jeffery, S., Mortimer, P.S., Mansour, S., and Ostergaard, P. (2013). The classification and diagnostic algorithm for primary lymphatic dysplasia: an update from 2010 to include molecular findings. Clin. Genet. *84*, 303–314.

Coso, S., Zeng, Y., Opeskin, K., and Williams, E.D. (2012). Vascular endothelial growth factor receptor-3 directly interacts with phosphatidylinositol 3-kinase to regulate lymphangiogenesis. PLoS ONE *7*, e39558.

de Boer, J., Williams, A., Skavdis, G., Harker, N., Coles, M., Tolaini, M., Norton, T., Williams, K., Roderick, K., Potocnik, A.J., and Kioussis, D. (2003). Transgenic mice with hematopoietic and lymphoid specific expression of Cre. Eur. J. Immunol. *33*, 314–325.

Ding, B.S., Nolan, D.J., Butler, J.M., James, D., Babazadeh, A.O., Rosenwaks, Z., Mittal, V., Kobayashi, H., Shido, K., Lyden, D., et al. (2010). Inductive angiocrine signals from sinusoidal endothelium are required for liver regeneration. Nature *468*, 310–315.

Dumont, D.J., Jussila, L., Taipale, J., Lymboussaki, A., Mustonen, T., Pajusola, K., Breitman, M., and Alitalo, K. (1998). Cardiovascular failure in mouse embryos deficient in VEGF receptor-3. Science *282*, 946–949.

Engelhardt, B., and Liebner, S. (2014). Novel insights into the development and maintenance of the blood-brain barrier. Cell Tissue Res. *355*, 687–699.

Foo, S.S., Turner, C.J., Adams, S., Compagni, A., Aubyn, D., Kogata, N., Lindblom, P., Shani, M., Zicha, D., and Adams, R.H. (2006). Ephrin-B2 controls cell motility and adhesion during blood-vessel-wall assembly. Cell *124*, 161–173.

Ginhoux, F., Greter, M., Leboeuf, M., Nandi, S., See, P., Gokhan, S., Mehler, M.F., Conway, S.J., Ng, L.G., Stanley, E.R., et al. (2010). Fate mapping analysis reveals that adult microglia derive from primitive macrophages. Science *330*, 841–845.

Gordon, E.J., Rao, S., Pollard, J.W., Nutt, S.L., Lang, R.A., and Harvey, N.L. (2010). Macrophages define dermal lymphatic vessel calibre during development by regulating lymphatic endothelial cell proliferation. Development *137*, 3899–3910.

Graupera, M., and Potente, M. (2013). Regulation of angiogenesis by PI3K signaling networks. Exp. Cell Res. *319*, 1348–1355.

Graupera, M., Guillermet-Guibert, J., Foukas, L.C., Phng, L.K., Cain, R.J., Salpekar, A., Pearce, W., Meek, S., Millan, J., Cutillas, P.R., et al. (2008). Angiogenesis selectively requires the p110alpha isoform of PI3K to control endothelial cell migration. Nature *453*, 662–666.

Gupta, S., Ramjaun, A.R., Haiko, P., Wang, Y., Warne, P.H., Nicke, B., Nye, E., Stamp, G., Alitalo, K., and Downward, J. (2007). Binding of ras to phosphoinositide 3-kinase p110alpha is required for ras-driven tumorigenesis in mice. Cell *129*, 957–968.

Hägerling, R., Pollmann, C., Andreas, M., Schmidt, C., Nurmi, H., Adams, R.H., Alitalo, K., Andresen, V., Schulte-Merker, S., and Kiefer, F. (2013). A novel multistep mechanism for initial lymphangiogenesis in mouse embryos based on ultramicroscopy. EMBO J. *32*, 629–644.

Haiko, P., Makinen, T., Keskitalo, S., Taipale, J., Karkkainen, M.J., Baldwin, M.E., Stacker, S.A., Achen, M.G., and Alitalo, K. (2008). Deletion of vascular endothelial growth factor C (VEGF-C) and VEGF-D is not equivalent to VEGF receptor 3 deletion in mouse embryos. Mol. Cell. Biol. *28*, 4843–4850.

Hirschi, K.K. (2012). Hemogenic endothelium during development and beyond. Blood *119*, 4823–4827.

Huntington, G.S., and McClure, C.F.W. (1910). The anatomy and development of the jugular lymph sacs in the domestic cat (Felis domestica). Am. J. Anat. *10*, 177–312.

Karkkainen, M.J., Haiko, P., Sainio, K., Partanen, J., Taipale, J., Petrova, T.V., Jeltsch, M., Jackson, D.G., Talikka, M., Rauvala, H., et al. (2004). Vascular endothelial growth factor C is required for sprouting of the first lymphatic vessels from embryonic veins. Nat. Immunol. *5*, 74–80.

Kerjaschki, D., Huttary, N., Raab, I., Regele, H., Bojarski-Nagy, K., Bartel, G., Kröber, S.M., Greinix, H., Rosenmaier, A., Karlhofer, F., et al. (2006). Lymphatic endothelial progenitor cells contribute to de novo lymphangiogenesis in human renal transplants. Nat. Med. *12*, 230–234.

Kim, D.H., Cho, S., and Wirtz, D. (2014). Tight coupling between nucleus and cell migration through the perinuclear actin cap. J. Cell Sci. *127*, 2528–2541.

Klein, S., Seidler, B., Kettenberger, A., Sibaev, A., Rohn, M., Feil, R., Allescher, H.D., Vanderwinden, J.M., Hofmann, F., Schemann, M., et al. (2013). Interstitial cells of Cajal integrate excitatory and inhibitory neurotransmission with intestinal slow-wave activity. Nat. Commun. *4*, 1630.

Kusumbe, A.P., Ramasamy, S.K., and Adams, R.H. (2014). Coupling of angiogenesis and osteogenesis by a specific vessel subtype in bone. Nature *507*, 323–328.

Lapinski, P.E., Kwon, S., Lubeck, B.A., Wilkinson, J.E., Srinivasan, R.S., Sevick-Muraca, E., and King, P.D. (2012). RASA1 maintains the lymphatic vasculature in a quiescent functional state in mice. J. Clin. Invest. *122*, 733–747.

Lenard, A., Ellertsdottir, E., Herwig, L., Krudewig, A., Sauteur, L., Belting, H.G., and Affolter, M. (2013). In vivo analysis reveals a highly stereotypic morphogenetic pathway of vascular anastomosis. Dev. Cell *25*, 492–506.

Mäkinen, T., Jussila, L., Veikkola, T., Karpanen, T., Kettunen, M.I., Pulkkanen, K.J., Kauppinen, R., Jackson, D.G., Kubo, H., Nishikawa, S., et al. (2001a). Inhibition of lymphangiogenesis with resulting lymphedema in transgenic mice expressing soluble VEGF receptor-3. Nat. Med. *7*, 199–205.

Mäkinen, T., Veikkola, T., Mustjoki, S., Karpanen, T., Catimel, B., Nice, E.C., Wise, L., Mercer, A., Kowalski, H., Kerjaschki, D., et al. (2001b). Isolated lymphatic endothelial cells transduce growth, survival and migratory signals via the VEGF-C/D receptor VEGFR-3. EMBO J. *20*, 4762–4773.

Marcelo, K.L., Sills, T.M., Coskun, S., Vasavada, H., Sanglikar, S., Goldie, L.C., and Hirschi, K.K. (2013). Hemogenic endothelial cell specification requires c-Kit, Notch signaling, and p27-mediated cell-cycle control. Dev. Cell *27*, 504–515.

Maruyama, K., Ii, M., Cursiefen, C., Jackson, D.G., Keino, H., Tomita, M., Van Rooijen, N., Takenaka, H., D'Amore, P.A., Stein-Streilein, J., et al. (2005). Inflammation-induced lymphangiogenesis in the cornea arises from CD11b-positive macrophages. J. Clin. Invest. *115*, 2363–2372.

Mellor, R.H., Hubert, C.E., Stanton, A.W., Tate, N., Akhras, V., Smith, A., Burnand, K.G., Jeffery, S., Mäkinen, T., Levick, J.R., and Mortimer, P.S. (2010).

Lymphatic dysfunction, not aplasia, underlies Milroy disease. Microcirculation *17*, 281–296.

Mouta-Bellum, C., Kirov, A., Miceli-Libby, L., Mancini, M.L., Petrova, T.V., Liaw, L., Prudovsky, I., Thorpe, P.E., Miura, N., Cantley, L.C., et al. (2009). Organ-specific lymphangiectasia, arrested lymphatic sprouting, and maturation defects resulting from gene-targeting of the PI3K regulatory isoforms p85alpha, p55alpha, and p50alpha. Dev. Dyn. *238*, 2670–2679.

Muzumdar, M.D., Tasic, B., Miyamichi, K., Li, L., and Luo, L. (2007). A global double-fluorescent Cre reporter mouse. Genesis *45*, 593–605.

Nakano, H., Liu, X., Arshi, A., Nakashima, Y., van Handel, B., Sasidharan, R., Harmon, A.W., Shin, J.H., Schwartz, R.J., Conway, S.J., et al. (2013). Haemogenic endocardium contributes to transient definitive haematopoiesis. Nat. Commun. *4*, 1564.

Nolan, D.J., Ginsberg, M., Israely, E., Palikuqi, B., Poulos, M.G., James, D., Ding, B.S., Schachterle, W., Liu, Y., Rosenwaks, Z., et al. (2013). Molecular signatures of tissue-specific microvascular endothelial cell heterogeneity in organ maintenance and regeneration. Dev. Cell *26*, 204–219.

Ny, A., Koch, M., Schneider, M., Neven, E., Tong, R.T., Maity, S., Fischer, C., Plaisance, S., Lambrechts, D., Héligon, C., et al. (2005). A genetic Xenopus laevis tadpole model to study lymphangiogenesis. Nat. Med. *11*, 998–1004.

Oliver, G., and Srinivasan, R.S. (2010). Endothelial cell plasticity: how to become and remain a lymphatic endothelial cell. Development *137*, 363–372.

Phng, L.K., Stanchi, F., and Gerhardt, H. (2013). Filopodia are dispensable for endothelial tip cell guidance. Development *140*, 4031–4040.

Sabin, F.R. (1902). On the origin of the lymphatic system from the veins and the development of the lymph hearts and thoracic duct in the pig. Am. J. Anat. *1*, 367–389.

Salven, P., Mustjoki, S., Alitalo, R., Alitalo, K., and Rafii, S. (2003). VEGFR-3 and CD133 identify a population of CD34+ lymphatic/vascular endothelial precursor cells. Blood *101*, 168–172.

Sinha, S., Iyer, D., and Granata, A. (2014). Embryonic origins of human vascular smooth muscle cells: implications for in vitro modeling and clinical application. Cell. Mol. Life Sci. *71*, 2271–2288.

Srinivasan, R.S., Dillard, M.E., Lagutin, O.V., Lin, F.J., Tsai, S., Tsai, M.J., Samokhvalov, I.M., and Oliver, G. (2007). Lineage tracing demonstrates the venous origin of the mammalian lymphatic vasculature. Genes Dev. *21*, 2422–2432.

Stenman, J.M., Rajagopal, J., Carroll, T.J., Ishibashi, M., McMahon, J., and McMahon, A.P. (2008). Canonical Wnt signaling regulates organ-specific assembly and differentiation of CNS vasculature. Science *322*, 1247–1250.

van der Putte, S.C. (1975). The early development of the lymphatic system in mouse embryos. Acta Morphol. Neerl. Scand. *13*, 245–286.

Vanhaesebroeck, B., Guillermet-Guibert, J., Graupera, M., and Bilanges, B. (2010). The emerging mechanisms of isoform-specific PI3K signalling. Nat. Rev. Mol. Cell Biol. *11*, 329–341.

Wilting, J., Papoutsi, M., Schneider, M., and Christ, B. (2000). The lymphatic endothelium of the avian wing is of somitic origin. Dev. Dyn. *217*, 271–278.

Wilting, J., Aref, Y., Huang, R., Tomarev, S.I., Schweigerer, L., Christ, B., Valasek, P., and Papoutsi, M. (2006). Dual origin of avian lymphatics. Dev. Biol. *292*, 165–173.

Yang, Y., García-Verdugo, J.M., Soriano-Navarro, M., Srinivasan, R.S., Scallan, J.P., Singh, M.K., Epstein, J.A., and Oliver, G. (2012). Lymphatic endothelial progenitors bud from the cardinal vein and intersomitic vessels in mammalian embryos. Blood *120*, 2340–2348.

Cell Reports

Supplemental Information

cKit Lineage Hemogenic Endothelium-Derived Cells Contribute to Mesenteric Lymphatic Vessels

Lukas Stanczuk, Ines Martinez-Corral, Maria Ulvmar, Yang Zhang, Bàrbara Laviña, Marcus Fruttiger, Ralf H. Adams, Dieter Saur, Christer Betsholtz, Sagrario Ortega, Kari Alitalo, Mariona Graupera, and Taija Mäkinen

A

Stage	Genotype				
	Wt	*p110α*$^{D933A/+}$	*Vegfr3*$^{lz/+}$	*Vegfr3*$^{lz/+}$; *p110α*$^{D933A/+}$	Total
E13-E18	21 (21%)	31 (32%)	22 (22%)	25 (26%)	98
P0-P7	29 (34%)	31 (36%)	15 (17%)	11 (13%)	86
P21	4 (45%)	2 (22%)	3 (33%)	0 (0%)	9
Expected	25%	25%	25%	25%	

B

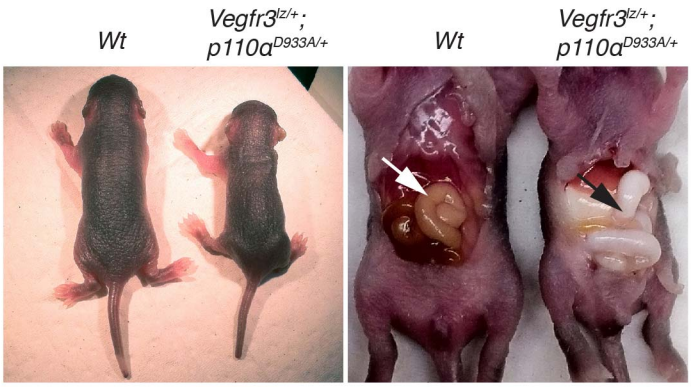

C

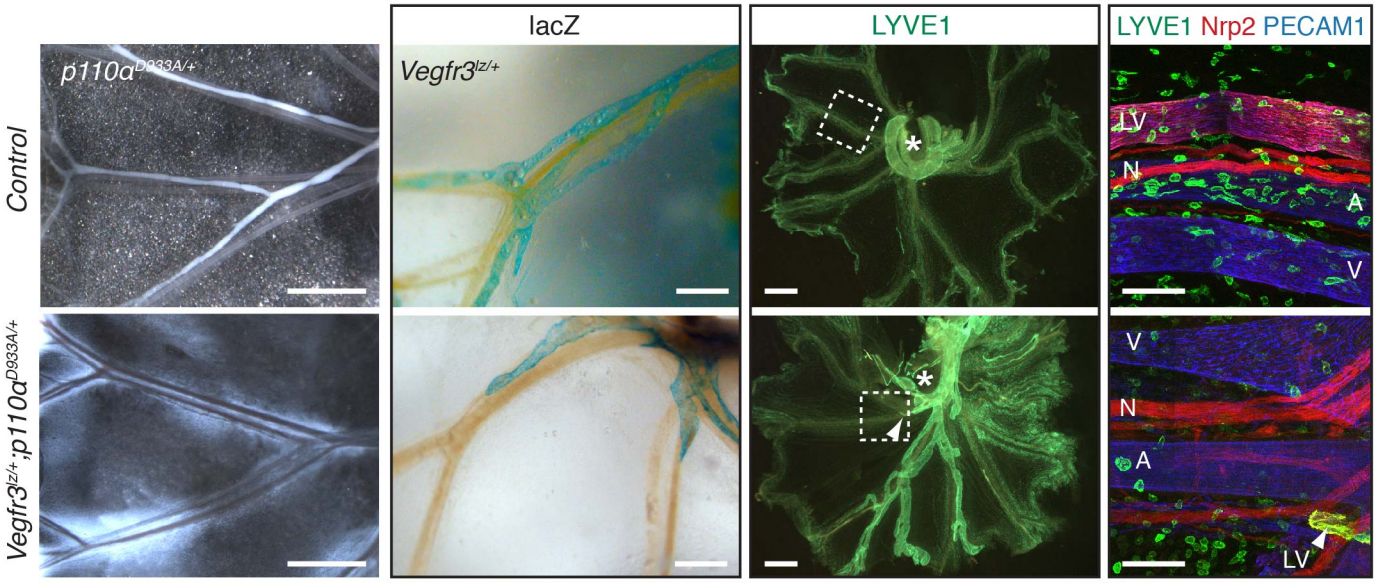

D

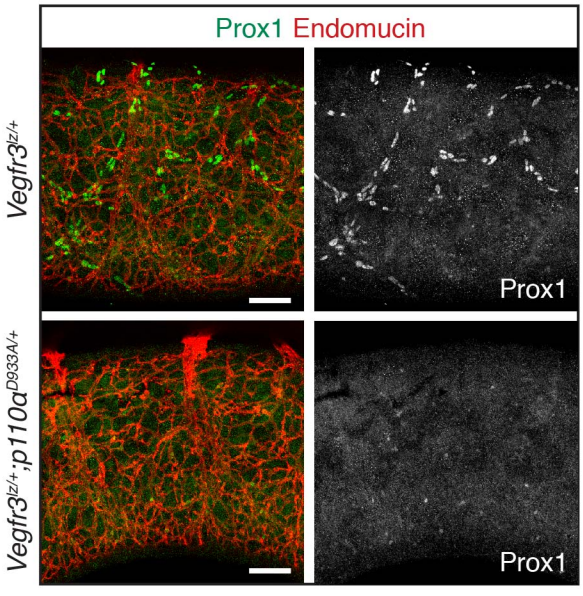

E

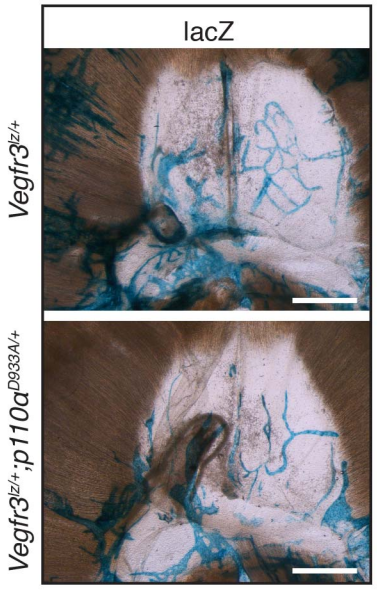

Figure S1

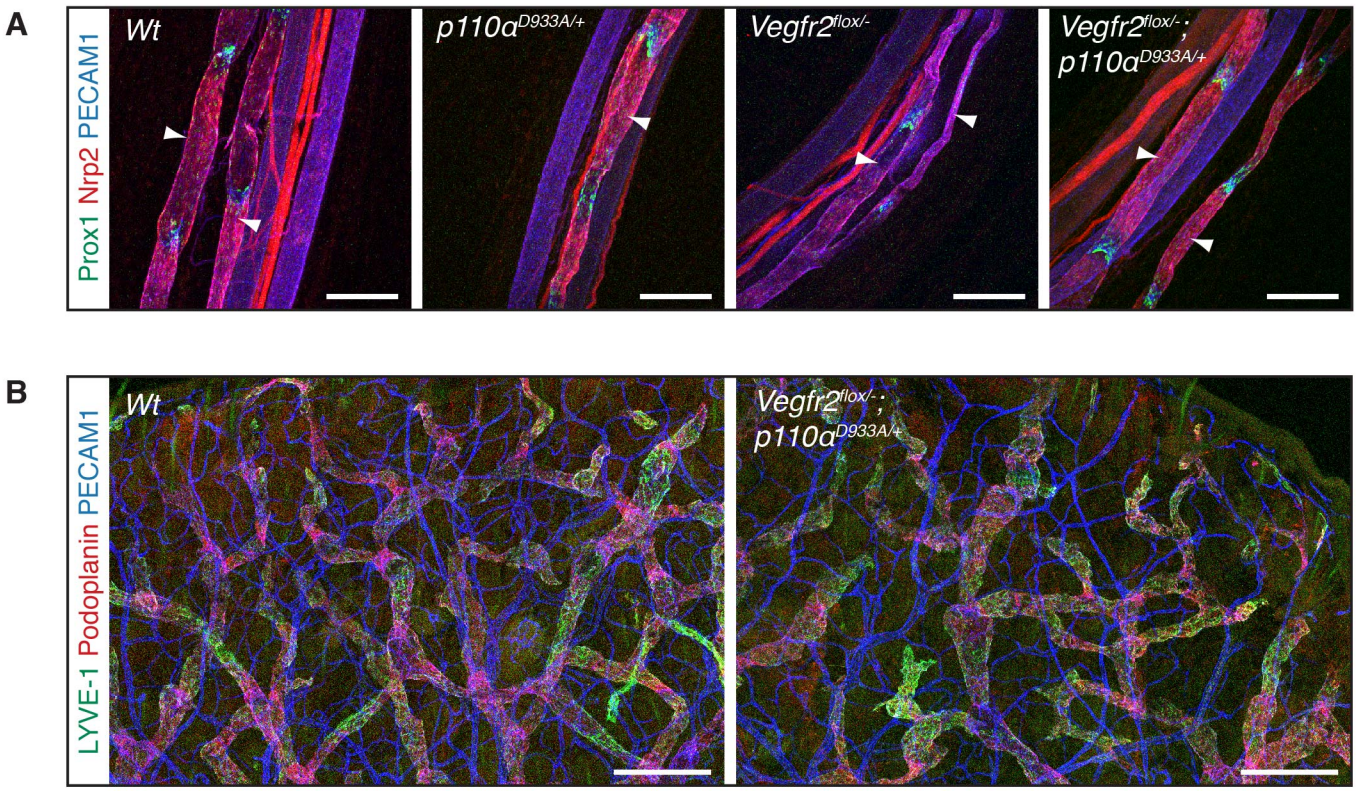
A
Prox1 Nrp2 PECAM1
Wt
p110α D933A/+
Vegfr2 flox/-
Vegfr2 flox/-; p110α D933A/+
B
LYVE-1 Podoplanin PECAM1
Wt
Vegfr2 flox/-; p110α D933A/+

Figure S2

A

FACS analysis of skin EC from E15.5 *Vegfr3-CreER^{T2};R26-mTmG*

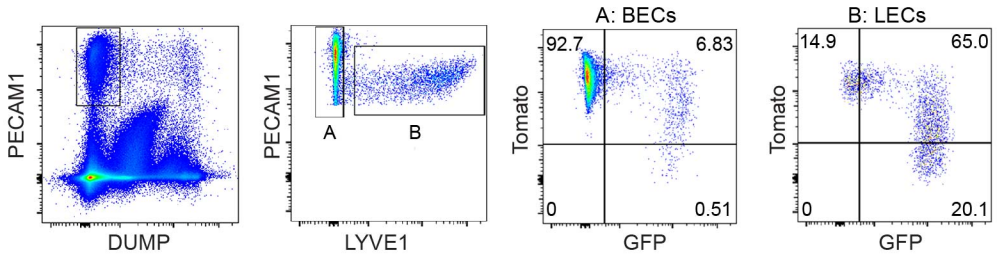

B

FACS analysis of mesenteries and intestinal ECs from E17.5 *Vegfr3-CreER^{T2};R26-mTmG*

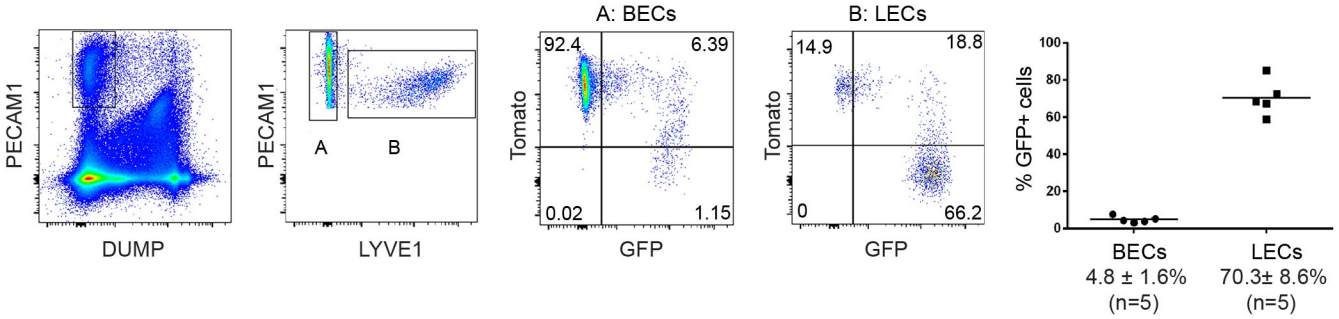

FACS analysis of skin EC from E17.5 *Vegfr3-CreER^{T2};R26-mTmG*

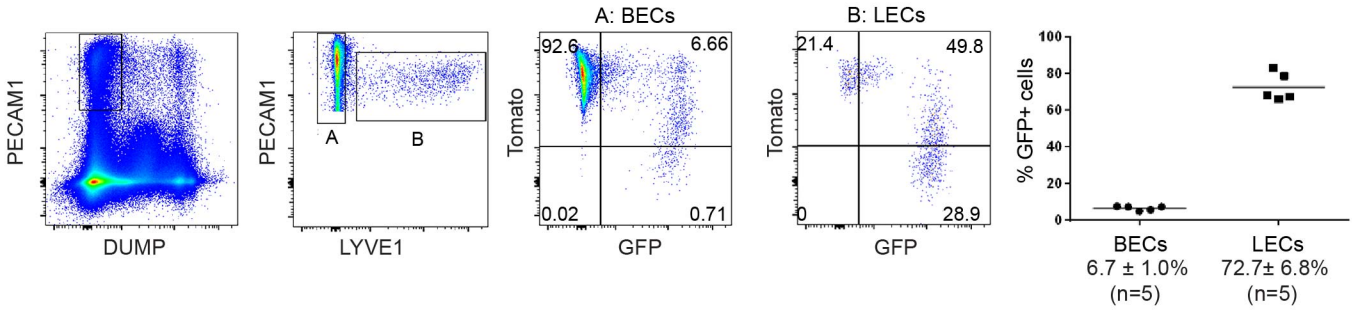

Figure S3

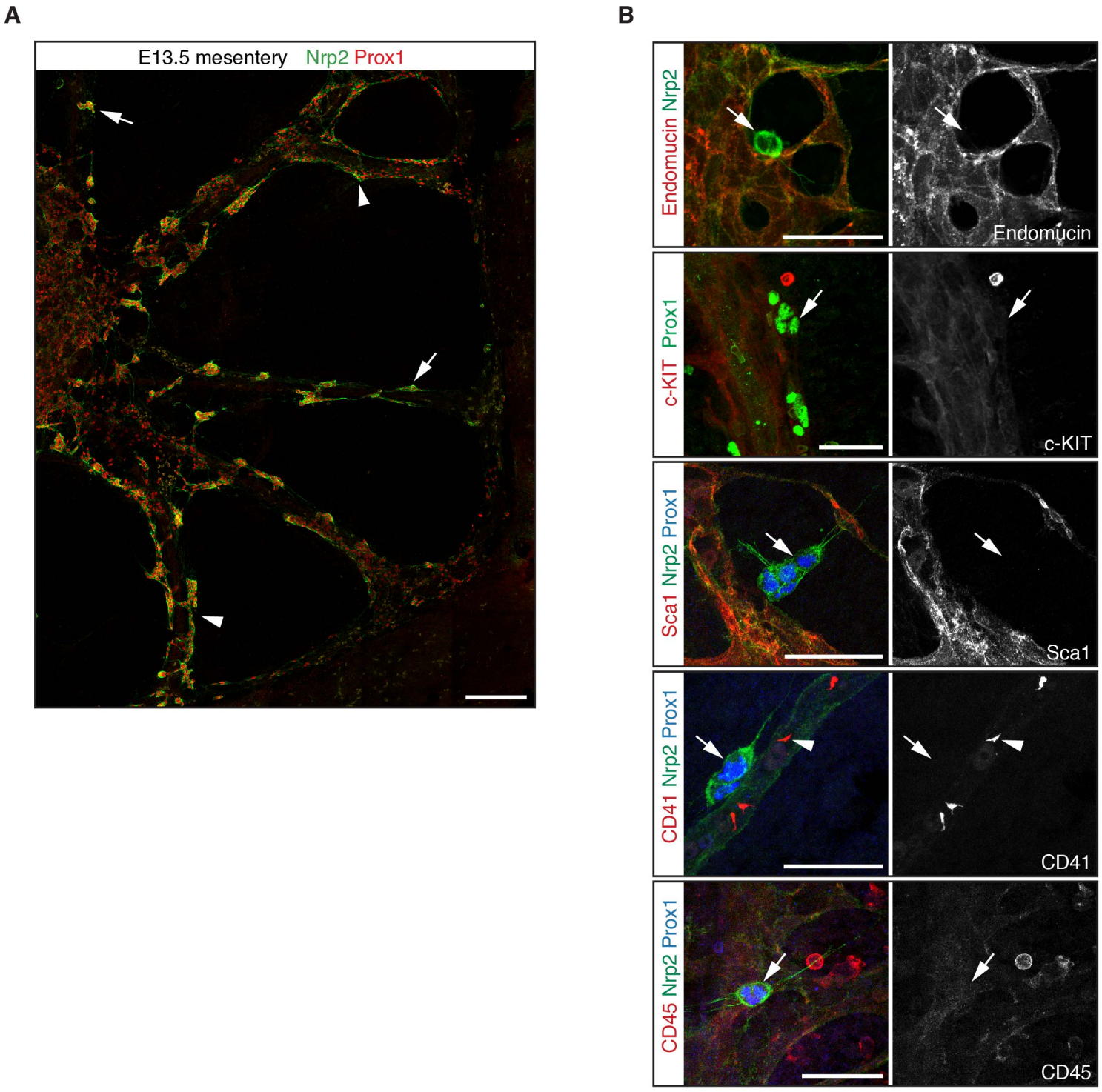
A
E13.5 mesentery Nrp2 Prox1
B
Endomucin Nrp2
Endomucin
c-KIT Prox1
c-KIT
Sca1 Nrp2 Prox1
Sca1
CD41 Nrp2 Prox1
CD41
CD45 Nrp2 Prox1
CD45

Figure S4

A

induction	GFP labeling in mesentery				number of		% embryos with LEC labeling
	artery	vein	lymphatic	HC	embryos	litters	
E8	(+)	-	- / + / ++	+++	4	2	50
E9	+++	+	- / +	++	3	2	67
E8+E9	+++	++	+ / ++	+++	3	3	100
E10	+++	+	+	(+)	2	2	100
E10+E11	+++	++	+	(+)	2	2	100
E11+E12	+++	++	(+)	- / (+)	3	3	100
E13	+++	++	(+)	-	2	1	100
E14	+++	++	(+)	-	2	1	100

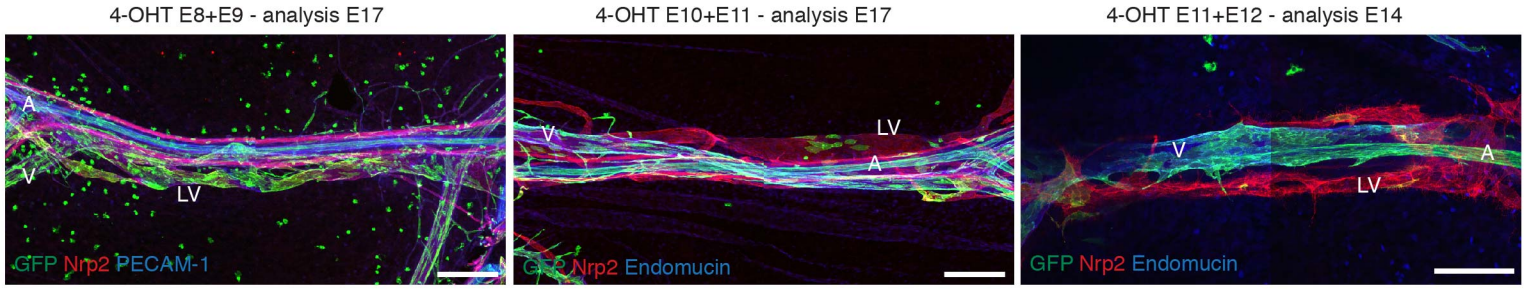

B FACS analysis of E11 *Pdgfb-CreER^{T2};R26-mTmG* whole embryo **induced at E8**

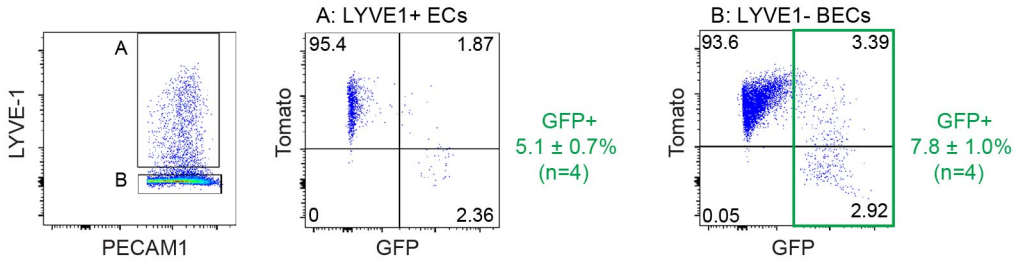

FACS analysis of E12 *Pdgfb-CreER^{T2};R26-mTmG* whole embryo **induced at E9**

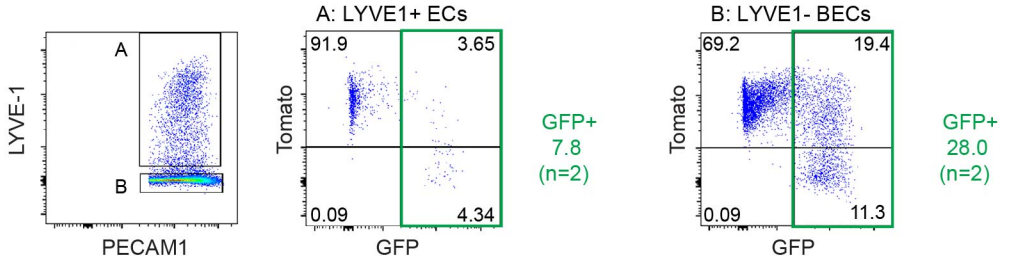

Figure S5

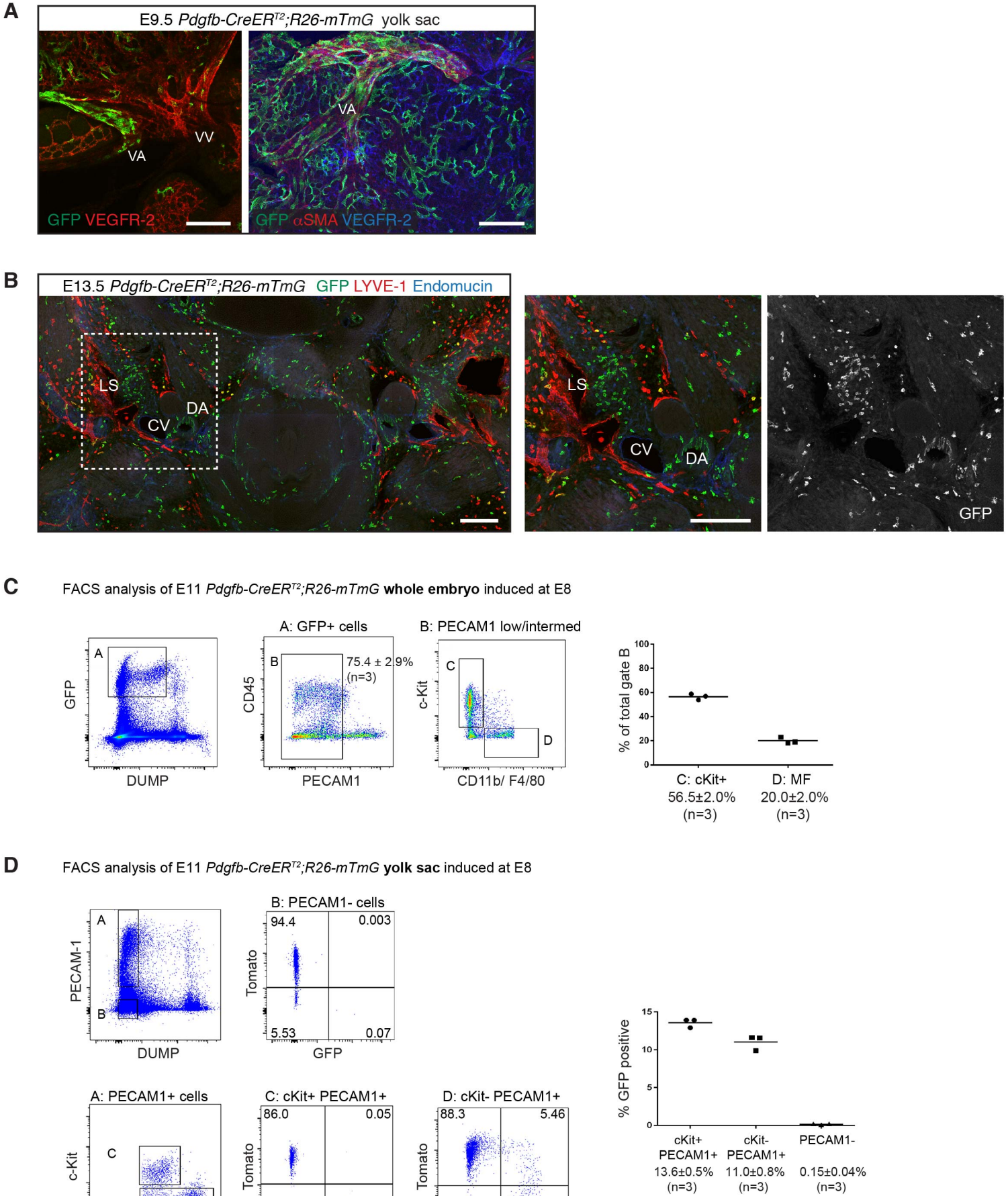
A
E9.5 Pdgfb-CreER^{T2};R26-mTmG yolk sac
VA
VV
GFP VEGFR-2
VA
GFP αSMA VEGFR-2
B
E13.5 Pdgfb-CreER^{T2};R26-mTmG GFP LYVE-1 Endomucin
LS
DA
CV
LS
CV
DA
GFP
C
FACS analysis of E11 Pdgfb-CreER^{T2};R26-mTmG whole embryo induced at E8
A: GFP+ cells
B: PECAM1 low/intermed
GFP
DUMP
CD45
PECAM1
75.4 ± 2.9%
(n=3)
c-Kit
CD11b/ F4/80
% of total gate B
C: cKit+
56.5±2.0%
(n=3)
D: MF
20.0±2.0%
(n=3)
D
FACS analysis of E11 Pdgfb-CreER^{T2};R26-mTmG yolk sac induced at E8
B: PECAM1- cells
PECAM-1
DUMP
Tomato
GFP
94.4
0.003
5.53
0.07
A: PECAM1+ cells
C: cKit+ PECAM1+
D: cKit- PECAM1+
c-Kit
PECAM1
86.0
0.05
0.11
13.8
88.3
5.46
0.13
6.14
% GFP positive
cKit+
PECAM1+
13.6±0.5%
(n=3)
cKit-
PECAM1+
11.0±0.8%
(n=3)
PECAM1-
0.15±0.04%
(n=3)

Figure S6

A

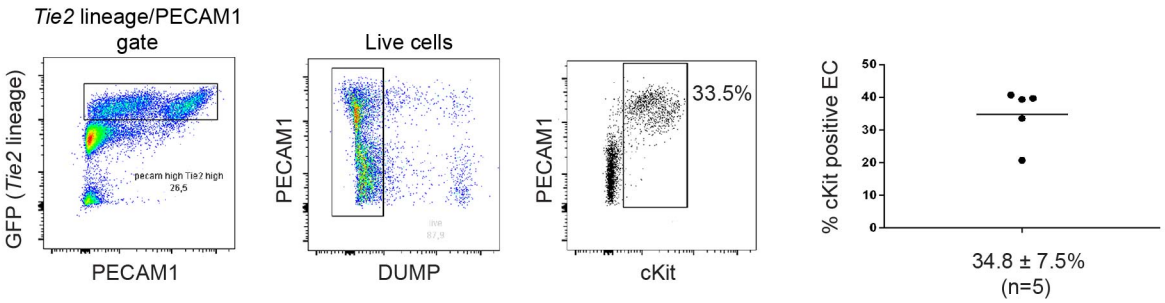
FACS analysis of E9 Tie2-Cre;R26-mTmG yolk sac
Tie2 lineage/PECAM1 gate
GFP (Tie2 lineage)
PECAM1
pecam high Tie2 high
26,5
Live cells
PECAM1
DUMP
PECAM1
33.5%
cKit
% cKit positive EC
50
40
30
20
10
0
34.8 ± 7.5%
(n=5)

B

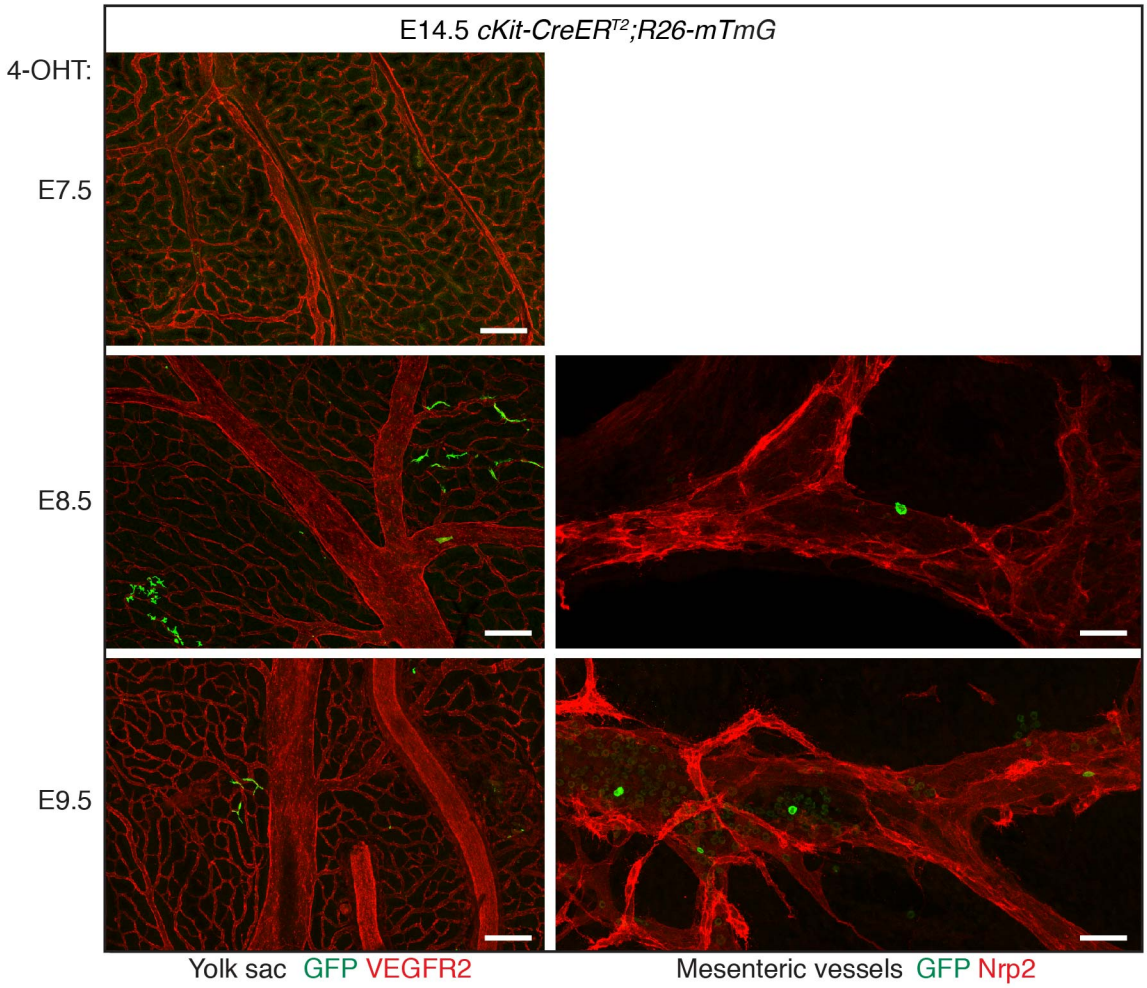
E14.5 cKit-CreER^T2;R26-mTmG
4-OHT:
E7.5
E8.5
E9.5
Yolk sac GFP VEGFR2
Mesenteric vessels GFP Nrp2

Figure S7

Supplemental Figure Legends

Figure S1, related to Figure 1. Perinatal lethality and selective inhibition of mesenteric lymphatic vessel development in *Vegfr3*$^{lz/+}$; *p110α*$^{D933A/+}$ mice.

(A) Observed and expected genotypes of embryos and mice from crosses of *p110α*$^{D933A/+}$ and *Vegfr3*$^{lz/+}$ mice. Double heterozygotes were recovered at expected Mendelian ratio before birth, but they died perinatally (highlighted in red). (B) *Vegfr3*$^{lz/+}$;*p110α*$^{D933A/+}$ pup and a wild type littermate (*Wt*) at P4. Note accumulation of chyle in the mutant intestine (arrows). (C) Mesenteries from P4 *Vegfr3*$^{lz/+}$; *p110α*$^{D933A/+}$ and littermate control mice. Lymphatic vessels were visualized by whole-mount X-Gal staining (lacZ, blue) or immunofluorescence for indicated proteins. Note diffuse leakage of chyle and rudimentary lymphatic vessels in the mesentery of mutant mice. Boxed regions show regions imaged on the right and asterisks indicate the mesenteric root. *Vegfr3*$^{lz/+}$; *p110α*$^{D933A/+}$ embryos develop only few mesenteric vessels that abnormally retain LYVE-1 expression. LV = lymphatic vessel, V = vein, A = artery, N = nerve. Scattered LYVE-1 cells are macrophages. (D) Whole-mount immunofluorescence of E17.5 intestine stained against indicated proteins. Single channel images for Prox1 are shown. (E) X-Gal stained diaphragms from P4 *Vegfr3*$^{lz/+}$; *p110α*$^{D933A/+}$ and littermate control mice showing grossly normal lymphatic network in the mutant.

Scale bars = 0.5 mm (C, left panel), 1 mm (C, middle panels; E), 100 μm (C, rightmost panel; D).

Figure S2, related to Figure 1. *Vegfr2*$^{flox/-}$;*p110α*$^{D933A/+}$ mice show no detectable phenotype in the lymphatic vasculature.

Whole-mount immunofluorescence of P4 mesenteric vasculature (A) and P21 dermal vasculature of the ear (B) stained with antibodies against indicated proteins. Arrowheads indicate lymphatic vessels.

Scale bars = 200 μm.

Figure S3, related to Figure 1. Cre-mediated recombination efficiency in the *Vegfr3-CreER*^{T2} line.

(A) FACS analysis of dermal endothelial cells from E15.5 *Vegfr3-CreER*^{T2}*;R26-mTmG* embryos showing GFP expression, indicating Cre recombination, in LECs and to a lesser extent in BECs. Representative FACS plots and gating scheme are shown and the graph of all results is shown in Figure 1E.

(B) FACS analysis of endothelial cells from E17.5 *Vegfr3-CreER*^{T2}*;R26-mTmG* mesenteries (top panels) and skin (bottom panels) showing GFP expression, indicating Cre recombination, in LECs and to a lesser extent in BECs. Representative FACS plots and gating scheme and the graph of all results are shown. The horizontal lines represent mean (n=5). For both (A) and (B) 4-OHT was administered at E10.5, E11.5, E12.5 and E13.5.

Figure S4, related to Figure 3. Characterization of mesenteric LEC clusters.

(A, B) Whole-mount immunofluorescence of E13.5 mesenteries stained with antibodies against the indicated proteins. Different stages of LEC cluster (arrows in A) and vessel formation (arrowheads in A) are observed along different artery-vein pairs within the same mesentery. Arrows in (B) indicate isolated LEC clusters negative for blood endothelial and hematopoietic markers. Arrowhead in (B) indicates CD41^{+} platelets.

Scale bars = 200 μm (A), 50 μm (B).

Figure S5, related to Figure 4. Time-course of 4-OHT induced *Pdgfb-CreER^{T2}* mediated recombination in embryonic vasculature.

(A) Time-course of 4-OHT induced Cre-mediated recombination efficiency in vascular and hematopoietic cells in *Pdgfb-CreER^{T2};R26-mTmG* mesenteries. Relative recombination efficiency in different compartments was assessed through visual scoring: +++ extensive/complete, ++ good, + poor, (+) only a few GFP^{+} cells, - no GFP^{+} cells. HC = hematopoietic cells. Note a shift in the timing of 4-OHT administration when different vessel types/HCs are most efficiently targeted; early (<E9) administration leads to efficient labeling of LECs and HCs (highlighted in red) while later (>E10) administration leads to efficient labeling of arteries and veins. Representative images of mesenteries, stained for indicated proteins, for three 4-OHT administration regimes are shown below. LV = lymphatic vessels, V = vein, A = artery.

(B) FACS analysis of endothelial cells from E11 *Pdgfb-CreER^{T2};R26-mTmG* embryos treated with 4-OHT at E8 (top panels) or E9 (bottom panels). Representative FACS plots and gating scheme are shown. Summary of results showing increased recombination efficiency in both BECs and venous-derived LECs at E9 is presented on the right side of each FACS plot. Low level of GFP expression driven by *ires-GFP* within the *Pdgfb-CreER^{T2}* transgene is detected in the BECs. Only cells expressing high levels of GFP, indicating expression from the *R26-mTmG* reporter, are included in the analysis.

Scale bars = 100 μm.

Figure S6, related to Figure 4. Characterization of Cre recombination pattern in *Pdgfb-CreER^{T2};R26-mTmG* embryos treated with 4-OHT at E8-E8.5.

(A) Whole-mount immunofluorescence of E9 *Pdgfb-CreER^{T2};R26-mTmG* yolk sac for indicated proteins. Note efficient recombination indicated by GFP expression in the vitelline artery (VA) but not the vein (VV). The identity of VA was confirmed by staining for αSMA (on the right).

(B) Whole-mount immunofluorescence of a vibratome section from E13.5 *Pdgfb-CreER^{T2};R26-mTmG* embryo for indicated proteins. Recombination, indicated by GFP expression, can be seen in the dorsal aorta (DA) and hematopoietic cells, but not in the cardinal vein (CV; Endomucin^{+}) or lymph sac (LS; LYVE-1^{+}).

(C, D) FACS analysis of endothelial cells from E11 *Pdgfb-CreER^{T2};R26-mTmG* embryo proper (C) and yolk sac (D). In the embryo, *Pdgfb-CreER^{T2}* targets mainly cKit^{+} cells and macrophages (MF) (D). In the yolk sac Cre-mediated recombination occurs in both cKit^{+}/PECAM-1^{+} hemogenic and cKit^{-}/PECAM-1^{+} non-hemogenic endothelium, but not in PECAM-1^{-} non-endothelial cells (D). Representative FACS plots and gating schemes and graphs of all results are shown. The horizontal lines represent mean.

Scale bars = 200 μm.

Figure S7, related to Figure 5. cKit expression and *cKit-CreER^{T2}* mediated Cre recombination in the yolk sac.

(A) FACS analysis of yolk sac endothelial cells from E9.5 *Tie2-Cre;R26-mTmG* embryo. cKit expression in endothelial cells (gating based on the PECAM-1^{high}GFP^{+} cell profile) is analyzed. A representative FACS plot and gating scheme and graph of all results are shown. The horizontal line represents mean (n=5).

(B) Whole-mount immunofluorescence of E14.5 *cKit-CreER^{T2};R26-mTmG* yolk sacs and mesenteries for indicated proteins, showing low recombination efficiency indicated by a small number of GFP^{+} cells. 4-OHT was administered at E7.5, E8.5 or E9.5 as indicated. Scale bars = 200 μm (yolk sacs), 50 μm (mesenteries).

Supplemental Tables

Table S1. Image acquisition details for confocal micrographs

Figure	Panel	Tile	Max intensity proj	Objective
Figure 1A	mesenteric vessel	1 x 2	yes	Plan-Apochromat 20x/0.8 NA
	lymph sac	1 x 2	yes	Plan-Apochromat 20x/0.8 NA
	skin	2 x 4	yes	C-Apochromat 10x/0.45 NA
	diaphragm		yes	Plan-Apochromat 20x/0.8 Ph2
Figure 1F	mesenteric vessel		yes	Plan-Apochromat 20x/0.8 M27
Figure 1H		3 x 5	yes	Plan-Neofluar 10x/0.30 NA
Figure 2B	E12.5		yes	Plan-Apochromat 20x/0.8 Ph2
	E13.5	1 x 2	yes	Plan-Apochromat 20x/0.8 NA
	E14.5	1 x 2	yes	Plan-Apochromat 20x/0.8 NA
Figure 2C			yes	Plan-Apochromat 20x/0.8 NA
Figure 3A		1 x 2	yes	Plan-Apochromat 20x/0.8 NA
Figure 3B			yes	Plan-Apochromat 20x/0.8
Figure 3D	VEGFR2+Prox1		yes	C-Apochromat 40x/1.20 W Korr M27
	VEGFR3+Prox1		yes	C-Apochromat 40x/1.20 W Korr M27
	Nrp2+Prox1		yes	C-Apochromat 40x/1.20 W Korr M27
	Podoplanin+Prox1		yes	Plan-Apochromat 20x/0.8
	Nrp2+Edu+Prox1		yes	C-Apochromat 40x/1.20 W Korr M27
Figure 3E			yes	Plan-Apochromat 20x/0.8
Figure 3F			yes	Plan-Apochromat 20x/0.8
Figure 3G	whole mesentery	3 x 3	yes	Plan Apochromat 10x/0.45 M27
	lymph sac		yes	Plan-Apochromat 20x/0.8
	LEC cluster		yes	Plan-Apochromat 20x/0.8
Figure 4B		1 x 2	yes	Plan-Apochromat 20x/0.8 NA
Figure 4D	whole embryo	4 x 5	yes	Plan Apochromat 10x/0.45 M27
	zoomed region		yes	Plan Apochromat 10x/0.45 M27
	section		yes	Plan Apochromat 10x/0.45 M27
Figure 5B		1 x 2	yes	Plan-Apochromat 20x/0.8 NA
Figure 5C			yes	C-Apochromat 40x/1.20 W Korr M27
Figure 6A			no	C-Apochromat 40x/1.20 W Korr M27
Figure 6C	whole mesentery	3 x 3	yes	Plan-Neofluar 10x/0.30 NA
	mesenteric vessels	1 x 2	yes	Plan-Apochromat 20x/0.8 NA
	lymph sac	2 x 2	yes	Plan Apochromat 10x/0.45 M27
	skin	2 x 4	yes	Plan-Neofluar 10x/0.30 NA
Figure S1C	mesenteric vessels		yes	Plan-Apochromat 20x/0.8
Figure S1D			yes	Plan-Apochromat 20x/0.8
Figure S2A			yes	C-Apochromat 10x/0.45 W M27
Figure S2B		3 x 2	yes	Plan-Neofluar 10x/0.30 NA
Figure S4A		7 x 6	yes	Plan-Apochromat 20x/0.8 NA
Figure S4B	Endomucin+Nrp2		yes	C-Apochromat 40x/1.20 W Korr M27
	cKit+Prox1		yes	Plan-Apochromat 20x/0.8
	ScaI+Nrp2+Prox1		yes	C-Apochromat 40x/1.20 W Korr M27
	CD41+Nrp2+Prox1		yes	C-Apochromat 40x/1.20 W Korr M27
	CD45+Nrp2+Prox1		yes	C-Apochromat 40x/1.20 W Korr M27
Figure S5A	4OHT E8+E9	1 x 2	yes	Plan-Neofluar 10x/0.30
	4OHT E10+E11	1 x 2	yes	Plan-Neofluar 10x/0.30
	4OHT E11+E12	1 x 2	yes	Plan-Apochromat 20x/0.8 Ph2
Figure S6A	left		yes	Plan Apochromat 10x/0.45 M27
	right	2 x 2	yes	Plan Apochromat 10x/0.45 M27
Figure S6B		2 x 4	yes	Plan Apochromat 10x/0.45 M27
Figure S7B	yolk sacs	3 x 2	yes	Plan-Apochromat 10x/0.45 M27
	mesenteric vessels	1 x 2	yes	Plan-Apochromat 20x/0.8 NA

Supplemental Experimental Procedures

Mice

R26-mTmG (Muzumdar et al., 2007) mice were obtained from the Jackson Laboratory. *Vegfr3-CreER^{T2}* (I.M-C. and S.O., unpublished) will be published elsewhere. Transgenic mouse expressing EGFP under the control of the Claudin5 promoter/enhancer (*Cldn5-GFP*) was generated by B.L. and C.B. (unpublished). *Tie2-Cre* (Koni et al., 2001), *Pdgfb-CreER^{T2}* (Claxton et al., 2008), *cKit-CreER^{T2}* (Klein et al., 2013), *Pdgfrb-Cre* (Foo et al., 2006), *Vav-Cre* (de Boer et al., 2003), *Vegfr3^{flox}* (Haiko et al., 2008), *Vegfr3^{lz}* (Dumont et al., 1998), *p110α^{flox}* (Graupera et al., 2008) and *p110α^{D933A}* (Foukas et al., 2006) lines have been described previously. *Vegfr3$^{lz/+}$;p110α$^{D933A/+}$* embryos and pups were generated from crosses of heterozygous parents. *Vegfr2$^{+/-}$* mice were generated by crossing *Vegfr2^{flox}* (Haigh et al., 2003) with the *PGK-Cre* mice, followed by crossing with C57BL/6J mice to remove the Cre transgene. *Vegfr2$^{flox/-}$;p110α$^{D933A/+}$* embryos and pups were generated from crosses of *Vegfr2$^{+/-}$;p110α$^{D933A/+}$* and *Vegfr2$^{flox/flox}$* mice.

Antibodies

The following antibodies were used for immunofluorescence: rabbit anti-GFP (Invitrogen), hamster anti-mouse Podoplanin (Developmental Studies Hybridoma Bank), rabbit anti-human Prox1 (generated against human Prox1 C-terminus (567-737aa), Prox1-GST construct provided by Dr. T. Petrova, University of Lausanne), rat anti-mouse Endomucin (Santa Cruz Biotechnology), chicken anti-GFP, rat anti-mouse CD45, rat anti-mouse SCA1 (all from Abcam), rat anti-mouse PECAM-1, rat anti-mouse CD41, rat anti-mouse CD34 (all from

BectonDickinson), rat anti-mouse LYVE-1, goat anti-mouse c-KIT, goat anti-mouse Nrp2, goat anti-mouse VEGFR-2, goat anti-mouse VEGFR-3 (all from R&D Systems). Secondary antibodies conjugated to DyLight 405, Cy2, Cy3 or Cy5 were obtained from Jackson ImmunoResearch.

For FACS analysis, skin samples were stained with anti-LYVE-1 (ALY7) eF660 and anti-CD31/PECAM-1 (390) PE-Cy7, (both eBioscience). For E13 mesenteries, rat-anti podoplanin eF660 (eBio8.1.1) (eBioscience) was also added, to allow detection of non-LYVE1 positive LECs. Dump channel included anti-CD45 (30-F11) e450, anti-F4/80 (BM8) e450, anti-TER-119 (TER-119) eF450, anti-CD11b (M1/70) eF450 (all eBioscience) to exclude non-stromal cells and Sytox blue (Life technologies) to exclude non-viable cells. Yolk sacs and embryos were stained with different combinations of anti-CD31/PECAM-1 (390) PE-Cy7, anti-LYVE-1 (ALY7) eF660, anti-CD117 (2B8) APC or PERCP-eF710, anti-CD45 (30-F11) PERCP-Cy5.5. The dump channel included anti-F4/80 (BM8) eF450, anti-CD11b (M1/70) eF450, anti-TER-119 (TER-119) eF450 (all eBioscience) to exclude macrophages and red blood cells, together with Sytox blue (Life technologies) to exclude non-viable cells.

Quantification

Mesenteric lymphatic vessel phenotype was quantified by counting the proportion of artery-vein pairs (n=3-6 per embryo) extending from the mesenteric root to the intestine that were accompanied by lymphatic vessel(s) and presented as lymphatic vessel coverage: absent (no lymphatic vessels), <50% (less than half), ≥50% (more than half) and 100% (all artery-vein pairs accompanied by lymphatic vessel). Only continuous vascular structures connected to

the mesenteric root were considered as vessels. Control mice and embryos showed 100% coverage. The presence and size of the mesenteric lymph sac (absent, reduced size, normal size) was determined by comparison to littermate controls. Unless specified otherwise, controls represent littermate mice and embryos from different genotypes (single heterozygous, Cre-negative or wild type) that did not show a phenotype and were grouped.

Quantification of lymphatic vessel sprouting was done using LSM Image Browser (Zeiss) from maximum intensity projection images of tile scanned E17.5 skins (xy = 3400 µm x 1700 µm, upper thoracic region). The length of the sprout was calculated in relation to the dorsal midline. Dorsal midline was marked with a line. A distance of 1352 µm was measured laterally from the midline and the sprouting distance was calculated from the laterally located line to vessel tip. From each image 6-8 measurements were taken, 3-4 on each side of the midline. Quantification of lymphatic vessel branching was done from maximum intensity projection images of tile scanned E15.5 skins (xy = 3400 µm x 1700 µm, upper thoracic region) stained for Nrp2. All branch points per each image were marked using Photoshop CS5.1 software and counted manually.

For quantification of nuclear morphology the length/width ratio was measured for each $Prox1^+$ nuclei using ImageJ software. A total of 135 $Prox1^+$ cells were analyzed from lymphatic clusters (n=5 embryos), 123 from lymph sacs (n=2 embryos) and 141 from lymphatic vessels (n=5 embryos). For *Pdgfrb-Cre* lineage tracing, the number of GFP^+Prox1^+ cells versus all $Prox1^+$ cells within isolated LEC clusters was counted manually (n=24 clusters containing 2-12 cells each, from 3 embryos).

Quantification of GFP fluorescence intensity in endothelial cells of *Cldn5-GFP* mesenteries

was done using ImageJ software. Three measurements per cell were taken using the point tool and mean value was calculated. Background intensity value was similarly measured in each image and subtracted from the cell measurements. Total number of $Prox1^{+}$ cells measured was 27 (single cells), 23 (clusters of 2 cells), 38 (clusters of 3-4 cells) from 3 embryos.

In vivo cell proliferation assay

Click-iT Edu Imaging Kit (Invitrogen) was used to detect proliferating cells. Pregnant females were administered with 0.7 mg of Edu in PBS by intraperitoneal injection 5 hours prior to embryo dissection. Embryonic mesenteries were dissected, fixed, permeabilized and blocked with 3% milk in PBSTx as described above. Tissue was washed in PBS for 10 minutes at RT and incubated in the Click-iT reaction cocktail for 1 hour at room temperature followed by washes in PBS and staining with primary and secondary antibodies as described previously.

Detection of β-galactosidase activity by X-gal staining

The mesentery and diaphragm from *Vegfr3*$^{lz/+}$ mice were dissected and rinsed in 0.1M sodium phosphate buffer (pH 7.3) followed by incubation in the fixative (94mM sodium phosphate buffer pH 7.3 with 0.2% glutaraldehyde, 5mM EGTA pH 7.3, 2mM MgCl2,) for 30 minutes at RT. The tissues were washed three times in the wash buffer (0.1M sodium phosphate buffer pH 7.3 with 2mM MgCl2, 0.01% w/v deoxycholic acid, 0.02% NP-40) for 15 minutes each time at RT. Tissues were stained in X-gal staining solution (0.1% w/v X-gal, 0.212% w/v potassium ferrocyanide, 0.164% w/v potassium ferricyanide, in wash buffer)

overnight at 37°C. The following day, stained tissues were washed three times in the wash buffer for 15 minutes each time at RT then post-fixed in 4% PFA for approximately 8 hours at 4°C and stored in PBS at 4°C.

References

Claxton, S., Kostourou, V., Jadeja, S., Chambon, P., Hodivala-Dilke, K., and Fruttiger, M. (2008). Efficient, inducible Cre-recombinase activation in vascular endothelium. Genesis *46*, 74-80.

de Boer, J., Williams, A., Skavdis, G., Harker, N., Coles, M., Tolaini, M., Norton, T., Williams, K., Roderick, K., Potocnik, A.J.*, et al.* (2003). Transgenic mice with hematopoietic and lymphoid specific expression of Cre. Eur J Immun *33*, 314-325.

Dumont, D.J., Jussila, L., Taipale, J., Lymboussaki, A., Mustonen, T., Pajusola, K., Breitman, M., and Alitalo, K. (1998). Cardiovascular failure in mouse embryos deficient in VEGF receptor-3. Science *282*, 946-949.

Foo, S.S., Turner, C.J., Adams, S., Compagni, A., Aubyn, D., Kogata, N., Lindblom, P., Shani, M., Zicha, D., and Adams, R.H. (2006). Ephrin-B2 controls cell motility and adhesion during blood-vessel-wall assembly. Cell *124*, 161-173.

Foukas, L.C., Claret, M., Pearce, W., Okkenhaug, K., Meek, S., Peskett, E., Sancho, S., Smith, A.J., Withers, D.J., and Vanhaesebroeck, B. (2006). Critical role for the p110alpha phosphoinositide-3-OH kinase in growth and metabolic regulation. Nature *441*, 366-370.

Graupera, M., Guillermet-Guibert, J., Foukas, L.C., Phng, L.K., Cain, R.J., Salpekar, A., Pearce, W., Meek, S., Millan, J., Cutillas, P.R.*, et al.* (2008). Angiogenesis selectively

requires the p110alpha isoform of PI3K to control endothelial cell migration. Nature *453*, 662-666.

Haigh, J.J., Morelli, P.I., Gerhardt, H., Haigh, K., Tsien, J., Damert, A., Miquerol, L., Muhlner, U., Klein, R., Ferrara, N.*, et al.* (2003). Cortical and retinal defects caused by dosage-dependent reductions in VEGF-A paracrine signaling. Dev Biol *262*, 225-241.

Haiko, P., Makinen, T., Keskitalo, S., Taipale, J., Karkkainen, M.J., Baldwin, M.E., Stacker, S.A., Achen, M.G., and Alitalo, K. (2008). Deletion of vascular endothelial growth factor C (VEGF-C) and VEGF-D is not equivalent to VEGF receptor 3 deletion in mouse embryos. Mol Cell Biol *28*, 4843-4850.

Klein, S., Seidler, B., Kettenberger, A., Sibaev, A., Rohn, M., Feil, R., Allescher, H.D., Vanderwinden, J.M., Hofmann, F., Schemann, M.*, et al.* (2013). Interstitial cells of Cajal integrate excitatory and inhibitory neurotransmission with intestinal slow-wave activity. Nat Commun *4*, 1630.

Koni, P.A., Joshi, S.K., Temann, U.A., Olson, D., Burkly, L., and Flavell, R.A. (2001). Conditional vascular cell adhesion molecule 1 deletion in mice: impaired lymphocyte migration to bone marrow. J Exp Med *193*, 741-754.

Muzumdar, M.D., Tasic, B., Miyamichi, K., Li, L., and Luo, L. (2007). A global double-fluorescent Cre reporter mouse. Genesis *45*, 593-605.